Establishing Lagrangian connections between observations within air masses crossing the Atlantic during the ICARTT experiment

J. Methven,[1] S. R. Arnold,[2] A. Stohl,[3] M. J. Evans,[2] M. Avery,[4] K. Law,[5] A. C. Lewis,[6] P. S. Monks,[7] D. Parrish,[8] C. Reeves,[9] H. Schlager,[10] E. Atlas,[11] D. Blake,[12] H. Coe,[13] R. C. Cohen,[12] J. Crosier,[13] F. Flocke,[14] J. S. Holloway,[8] J. R. Hopkins,[6] G. Hübler,[8] J. McQuaid,[2] R. Purvis,[15] B. Rappenglück[16] T. B. Ryerson,[8] G. W. Sachse,[4] H. Singh,[17] N. Watson,[6] L. K. Whalley,[18] P. Williams[13]

Abstract. The ICARTT-Lagrangian experiment was conceived with an aim to quantify the effects of photochemistry and mixing on the transformation of air masses in the free troposphere away from emissions. To this end attempts were made to intercept and sample air masses several times during their journey across the North Atlantic using four aircraft based in New Hampshire (USA), Faial (Azores) and Creil (France). This article begins by describing forecasts using two Lagrangian models that were used to direct the aircraft into target air masses. A novel technique is then used to identify Lagrangian matches between flight segments. Two independent searches are conducted: for Lagrangian model matches and for pairs of whole air samples with matching hydrocarbon fingerprints. The information is filtered further by searching for matching hydrocarbon samples that are linked by matching trajectories. The quality of these "coincident matches" is assessed using temperature, humidity and tracer observations. The technique pulls out five clear Lagrangian cases covering a variety of situations and these are examined in detail. The matching trajectories and hydrocarbon fingerprints are shown and the downwind minus upwind differences in tracers are discussed.

1. Introduction to the ICARTT-Lagrangian Experiment

1.1. Why was a Lagrangian experiment needed?

Simulations of global atmospheric composition, designed to investigate climate change and air quality issues, rely on numerical models of transport and photochemistry. However, the chemical component of such models is uncertain, not only because its parameters are uncertain but also because chemical reaction mechanisms are reduced to make the problem tractable. Observations along a single flight are insufficient to evaluate the chemistry model because uncertainties in the origins of air masses dominate the uncertainty in modelled composition [*Methven et al.*, 2003]. This motivated the ambitious ICARTT (International Consortium for Atmospheric Research on Transport and Transformation) Lagrangian experiment (summer 2004) [see overview by *Fehsenfeld* [2006]] which aimed to track polluted air masses and intercept them several times as they crossed the Atlantic – time for observable photochemical transformation and mixing of air masses without experiencing further emissions.

A few Lagrangian experiments have been conducted previously. Notably, the Atlantic Stratocumulus Transition Experiment [ASTEX, *Huebert et al.* [1996]] and Aerosol Characterisation Experiments [ACE-1, *Bates et al.* [1998] and ACE-2, *Raes et al.* [2000]] measured changes in aerosol properties following air masses within the marine boundary layer. Three Lagrangian cases were observed during ACE-2 [*Johnson et al.*, 2000]. Air masses were tracked from near Portugal towards the Canary Islands using "smart" balloons travelling at constant altitude within the boundary layer. The physical and chemical properties of the surrounding air mass were intensively measured using the UK C-130 aircraft by intercepting the location of the balloon on three consecutive 9 hour flights (separated by only 3 hours), using forecast trajectories to determine the search area. The air masses were followed for 30 hours in each case. *Hoell et al.* [2000] conducted a time-scale analysis for the first and second ACE-2 Lagrangian cases and found that meteorological effects (boundary layer entrainment and surface wind speed) and physical aerosol-cloud interactions had greatest influence over the aerosol size distribution and number concentration and that the experiment time-scale was far too short for detecting chemical processing effects. In the third ACE-2 Lagrangian case the aerosol size distribution barely changed over 30 hours. *Fitzgerald et al.* [1998] estimated using a model that the evolution of aerosol from continental to marine air mass characteristics takes 6-8 days.

In the stratosphere, measurements from different balloon profiles have been linked using model trajectories [*Rex et al.* [1998]; *Lehmann et al.* [2005]] and ozonesonde launches have also been timed using trajectory forecasts to achieve Lagrangian matches. Such experiments can be described as "pseudo-Lagrangian" since an air mass is not tracked using a physical marker drifting with the wind (such as a balloon or tracer release), but observations are linked by trajectories derived using analysed wind fields. The quality of the Lagrangian links depends on the accuracy of the trajectory calculations and the closeness of sample points to the linking trajectories. A match is acceptable if the inferred changes in

ozone concentration following the air mass exceed the measurement errors and the "net match errors". *Lehmann et al.* [2005] showed that for the Match ozonesonde studies the net match errors are of similar magnitude to the measurement errors.

The ICARTT-Lagrangian 2K4 was carried out under the auspices of IGAC. It was the first experiment aiming to take measurements that were linked by trajectories over intercontinental distances through the free troposphere, where vertical motion is important. In the main, it can be described as a "pseudo-Lagrangian experiment" in that the "true trajectories" of air parcels will never been known. *Stohl et al.* [2004] have established such a Lagrangian link between measurements across the Atlantic during September 1997 between a flight of the NOAA (National Oceanic and Atmospheric Administration) WP-3D aircraft north from Newfoundland and a flight of the UK Meteorological Research Flight C-130 west of the Azores. In this case, the upwind aircraft was not deliberately aimed at targets forecast to be Lagrangian opportunities, although both aircraft were flying at the same time as part of the North Atlantic Regional Experiment (NARE) 97. The trajectories from the actual flight track of the WP-3D were also not forecast and therefore the link was somewhat fortuitous. The ICARTT-Lagrangian 2K4 aimed to maximise the chances for obtaining such links by forecasting Lagrangian opportunities and planning the flights on the basis of this information.

In addition, smart balloons were released into pollution plumes leaving the New England coast on a number of occasions and the surrounding air was sampled using aircraft over an interval of several days crossing the Gulf of Maine. *Riddle et al.* [2006] show that analysed trajectories follow the balloon tracks very closely, constituting a true Lagrangian experiment over a longer timescale than in ACE-2 [*Johnson et al.*, 2000].

1.2. Forecasting and flight coordination

During summer 2004, there was unprecedented coverage from observational platforms measuring atmospheric constituents, including measurements from aircraft, land-based sites and a ship and a new generation of satellite platforms [*Fehsenfeld*, 2006]. ICARTT formed an umbrella coordinating projects, each with differing objectives. ICARTT took advantage of this synergy by planning and executing a series of coordinated experiments to study aerosol and ozone precursors close to emissions and their subsequent chemical transformations and removal during transport. A key aim was to intercept a polluted air mass several times during its transit from North America across the Atlantic to investigate its chemical evolution in detail.

Four aircraft participated actively in the ICARTT-Lagrangian 2K4 experiment: the NOAA WP3-D, NASA (National Aeronautics and Space Administration) DC8, FAAM (Facility for Airborne Atmospheric Measurements) BAe146 and DLR (Deutsches Zentrum für Luft- und Raumfahrt) Falcon. There were two NOAA projects as part of ICARTT: ITCT (Intercontinental Transport and Chemical Transformation) and NEAQS (New England Air Quality Study). The NASA project was INTEX-NA (Intercontinental Chemical Transport Experiment - North America). The British and German/French projects were both named ITOP (Intercontinental Transport of Ozone and Precursors).

Detailed forecasts of the air mass trajectories from the East Coast USA were used to identify target air masses that would pass within range of the aircraft bases in Pease (New Hampshire, USA [43.09°N, 70.83°W]), Faial (Azores [38.52°N, 28.73°W]) and Creil (France [49.25°N, 2.51°E]). The two American aircraft (hereafter WP3-D and DC8) were directed through the targets by nudging flight plans associated with the other objectives of ICARTT [*Fehsenfeld*, 2006] to optimise the chance of air mass interception several days downwind. The forecasts were then refined by repeatedly calculating forward trajectories and Lagrangian plume calculations from their flight tracks (see Section 2) as the meteorological forecasts were updated. The primary goal of the two downwind aircraft (BAe146 and Falcon) was to intercept air that had been sampled close to North America.

One or two principal investigators from each aircraft platform participated daily in a conference call at 13:30 UTC. The aim was to coordinate the flights of the four aircraft from the USA, Azores and France where the local (summer) time was 09:30, 13:30 and 15:30 respectively. The calls were limited to 30 minutes. The order of discussion was: previous flights (key observations, problems), targets seen in forecasts ordered by place and time working downstream, and logistics for planning intercomparison flights.

Flights were also designed to link in with other measurements during ICARTT. For example, the WP3-D sampled upwind of the Chebogue Point site (Nova Scotia) where aerosol characterisation measurements were made. The BAe146 flew close by the NOAA observatory on the Pico volcano, before landing at Faial, whenever the top was cloud free, putting the aircraft observations into context with a multi-year record there [*Kleissl* [2006]; *Val Martin* [2006]]. Ground-based ozone lidar measurements were also collected during the campaign at sites in Europe, for example at Observatoire de Haute Provence in southern France [*Ravetta*, 2006].

Many chemical transport models were run in forecast mode for ICARTT. However, the detailed location of targets, identified as Lagrangian opportunities, relied on the

[1]Department of Meteorology, University of Reading, UK.
[2]School of Earth and Environment, University of Leeds, UK.
[3]Norwegian Institute for Air Research, Kjeller, Norway.
[4]NASA Langley RC, USA.
[5]Service d'Aéronomie/CNRS, Université Pierre et Marie Curie, Paris, France.
[6]Department of Chemistry, University of York, UK.
[7]Department of Chemistry, University of Leicester, UK.
[8]NOAA Aeronomy Laboratory, Boulder, CO, USA.
[9]School of Environmental Sciences, University of East Anglia, UK.
[10]DLR, Oberpfaffenhofen, Germany.
[11]Rosenstiel School of Marine and Atmospheric Science, University of Miami, USA.
[12]Department of Chemistry, University of California, USA.
[13]School of Earth, Atmospheric and Environmental Sciences, University of Manchester, UK.
[14]NCAR/ACD, Boulder, CO, USA.
[15]FAAM, Cranfield, UK.
[16]Institute of Meteorology and Climate Research, FZK, Garmisch-Partenkirchen, Germany.
[17]NASA Ames RC, Moffett Field, CA, USA.
[18]School of Chemistry, University of Leeds, UK.

Paper number .
0148-0227/06/$9.00

two Lagrangian models that will be discussed in Section 2. An example of the forecasts will be given.

1.3. Establishing Lagrangian links

This paper aims to identify successful Lagrangian links between aircraft observations and to infer the changes between upwind and downwind observations for the best Lagrangian cases. Following papers will examine the chemical and physical processes responsible for the changes by using Lagrangian models running along the matching trajectories. Matches are defined as occasions when a pair of whole air samples collected during different flights (WAS–pair) exhibit highly correlated hydrocarbon fingerprints and the sample time–windows are also connected by trajectories (calculated from meteorological analyses). The quality of the matches is evaluated using a third independent set of information: measurements of temperature and humidity combined into a single variable, the long–lived tracer equivalent potential temperature (θ_e). The statistics of ozone and carbon monoxide differences between upwind and downwind observations are presented.

Section 3 summarises the instruments and measurement techniques for observations utilised in this paper. Some salient results of the inter-comparison flights are also given here since these must be taken into account when estimating the uncertainty in chemical transformation inferred from upwind and downwind flights.

Section 4 explains the techniques used to identify matches using Lagrangian models and hydrocarbon fingerprints. Both sets of information are then used to infer coincident matches. The quality of the matches is assessed in Section 5 using probability density functions (PDFs) of the difference in observed tracer values upwind and downwind.

Section 6 analyses the best five Lagrangian cases from the ICARTT-Lagrangian experiment. The linking trajectories are shown, followed by their hydrocarbon fingerprints, composition and the inferred transformation between flights intercepting the air mass. The conclusions are presented in Section 7.

2. Lagrangian model forecasts

The essential processes represented in chemical/aerosol transport models are emissions, deposition, photochemical/microphysical transformation within air masses, transport of constituents by the winds and mixing between air masses by turbulence and convection. Above the boundary layer and outside regions of deep convection, the mixing timescale is generally much slower than advection timescales associated with stretching and folding of air masses by the large-scale winds (for fuller discussion see *Methven et al.* [2003]). Ozone is also long-lived in the sense that its photochemical timescale is long compared to the advection timescales [*Roelofs and Lelieveld*, 1997]. Consequently, air masses with distinct composition are stretched forming filaments on horizontal surfaces or layers on vertical profiles, with strong gradients in constituents at their edges [*Haynes and Anglade*, 1997].

Air masses rapidly become too narrow to resolve in global Eulerian models where the rate of change in concentration is considered at fixed grid points. This makes it difficult to compare the model simulations with observations and also implies much too great a mixing rate which can impact the chemical transformation if the reactions are nonlinearly dependent on concentration [*Esler et al.* [2001]; *Good et al.* [2003]; *Esler et al.* [2004]]. However, advection, mixing and transformation can be partitioned in different ways. Lagrangian trajectory models (Section 2.1) calculate the paths of air masses (often referred to as "particles" because they are assumed to be infinitesimally small) following the winds resolved in atmospheric analyses or forecasts. Transformation and mixing are then calculated together following trajectories. The main problem here is the lack of knowledge about the gradients between air masses and therefore mixing. Lagrangian dispersion models (Section 2.2) calculate the paths of particles following the resolved winds but also including a stochastic step to represent the effects of unresolved turbulence and convection [*Stohl et al.*, 2002]. The parameterised "random walk" shuffles particles, each weighted with the same tracer mass, so that their sum within a volume represents the effects of advection and diffusive mixing on passive tracer concentration [*Legras et al.*, 2003]. However, then the problem is that in this model framework a concentration is not associated with individual particles and mixing cannot affect chemical transformation along trajectories.

Although all three model types have their failings, both Lagrangian approaches are attractive because they deliberately partition the processes of transformation and mixing from the advection. The dynamics of the atmosphere also conspires to allow accurate simulation of tracer structures formed by advection on scales an order of magnitude finer than the resolution of the wind field [*Methven and Hoskins*, 1999]. The factor that limits the accuracy of simulation of concentrations, observed along aircraft flights for example, is uncertainty about the initial composition of air masses just after they have left the boundary layer, rather than transport simulation errors.

The aim of the ICARTT-Lagrangian experiment was to minimise the uncertainty associated with upwind composition by sampling there. Both types of Lagrangian models were used independently to forecast the paths of target air masses and in the identification of matches. The forecasts are described in the remainder of this section.

2.1. Trajectory model forecasts

The UGAMP (U.K. Universities Global Atmospheric Modelling Programme) trajectory model [*Methven* [1997]; *Methven et al.* [2003]] calculates trajectories, given wind fields and release coordinates, using a fourth order Runge-Kutta integration method. During ICARTT, the three wind components were calculated by transforming vorticity, divergence and surface pressure from the ECMWF (European Centre for Medium-Range Weather Forecasts) global spectral model truncated to T159 resolution on 60 hybrid–pressure η–levels. The transformation is identical to that used internally within the spectral model and the resulting winds were found on a Gaussian grid with spacing in longitude and latitude of approximately 1.125°. The winds at trajectory coordinates are found by cubic interpolation in the vertical and linear interpolation in the horizontal and time. Forecasts and analyses were spaced by time intervals of 6 hours and the trajectory time-step was one hour.

Domain filling trajectory forecasts were made backwards and forwards in time from 3D grids positioned over the East Coast USA and Azores, and backwards only from Western Europe. The "release grid" spacing was 0.75° in longitude,

0.50° in latitude and 25 hPa in pressure up to 200 hPa. The trajectory calculations were initiated immediately on completion of the latest ECMWF model forecast from 12UT. Trajectories were released from all grids at lead times of T+00, 24, 48 and 72 hours and also at lead times of 96 and 120 hours from the Azores and European grids. All trajectories were 7 days long except back trajectories from the US domain and forward trajectories from the Azores domain which were 3 days long. In total, 854144 trajectories were calculated following each daily meteorological forecast.

"Lagrangian opportunities" were identified by selecting the subset of trajectories from each grid that were forecast to pass within range of two or three of the aircraft bases (Pease, Faial and Creil). The useful operating range of the aircraft was defined to be 1000 km (although the DC8 has a much greater range). The subset was typically a small fraction of the whole set and was usually clustered into a few coherent ensembles of trajectories, enabling the plotting of all Lagrangian opportunies for a given grid and lead time on the same map. These plots (available from *http://badc.nerc.ac.uk/data/itop/*) were used for rapid selection of dates meriting further examination in each domain.

In order to identify Lagrangian opportunities that would also be likely to be polluted, emissions tracers were calculated. Gridded estimates of surface emissions were converted to volume sources by assuming instantaneous mixing throughout the depth of the boundary layer. Boundary layer depth was taken from the ECMWF model output. The sources were then integrated along trajectories whenever they were within the boundary layer. The NOx emissions inventory from the Emission Database for Global Atmospheric Research [EDGAR, *Olivier et al.* [1999]] was used to estimate the influence of anthropogenic emissions and the isoprene emissions inventory from *Guenther et al.* [1995] was used to indicate the influence of biogenic emissions (as a monthly mean). Clearly, both of these species have short lifetimes (less than a day) so the emissions tracers have much higher concentrations than could be observed along flights. Lagrangian opportunities were filtered on the basis

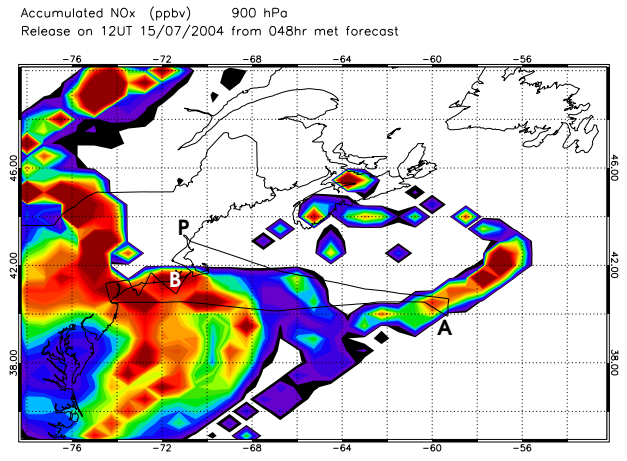

Figure 1. 48 hour forecast depicting NOx emissions tracer at 900 hPa in the US domain for the verification time 12UT 15 July 2004. A and B mark Lagrangian targets identified from the forecast. The flight track of the NOAA WP3-D aircraft from Pease, NH (point P) is overlain.

that the anthropogenic emissions tracer accumulated along back trajectories must exceed a threshold (10 ppbv) and the accumulated emissions along forward trajectories must stay below the same threshold. In this way, targets were identified with air masses leaving the continental boundary layer that would also pass within range of downwind aircraft.

Figure 1 shows an example of an emissions tracer forecast for the US East Coast domain for a verification time 12UT 15 July 2004, based on an ECMWF forecast starting from 12UT 13 July 2004. The Lagrangian opportunities mask showed that the air near points A and B was also forecast to pass within range of the Azores and Europe. The NOAA WP3-D aircraft was directed into targets A and B and the NASA DC8 also sampled air mass B on its descent into Pease.

Emissions tracers were also used to visualise the polluted air mass structure over the Atlantic. Typically the air masses are stretched and folded into thin, sloping sheets (e.g., Fig 12b). The forecasts were used to determine the best level to first intersect the target and select the shortest route to the target. Once intercepted the aircraft could be directed in the along–filament direction, sampling the air mass at several altitudes.

The target location was refined further by calculating trajectories forward from the actual flight track of the upwind aircraft. The coordinates were made available for the calculation within hours of landing. Trajectories were released every 10s along the tracks. This is sufficiently frequent that the locus of air mass locations from a target time-segment on the upwind flight can be followed downwind. The main displacement errors in trajectories are in the along-filament direction [*Methven and Hoskins*, 1999] so by flying through the forecast location of the target filament it is likely that air of similar composition will be sampled, even if the trajectory match has a displacement of tens of kilometres in the retrospective analysis.

Clearly, the forecast trajectories from flight tracks varied as the wind forecasts were updated, but qualitatively the set of trajectories retained similar shapes even though the first forecasts (for example 7 days forwards from T+72 hours into the meteorological forecast) are based on wind forecasts extending to very long lead times (10 days). On many occasions the targets sampled upwind drifted out of range of the downwind aircraft as the forecast lead time reduced, but in many cases the targets remained within range and were sampled (see Section 6 for the best cases).

2.2. Lagrangian dispersion model forecasts

During ICARTT forecasts were also made using FLEXPART, a Lagrangian particle dispersion model that simulates transport (by resolved winds), diffusion, dry and wet deposition. Details of the model are recorded in *Stohl et al.* [2005]. In its backwards in time (retroplume) mode, FLEXPART has been shown to simulate measurements of long-lived trace constituents at ground-based sites and along aircraft tracks to the extent that potential source contributions from different regions can be determined with some confidence [*Forster et al.* [2001]; *Stohl et al.* [2002]; *Stohl et al.* [2003]].

During the ICARTT period FLEXPART was run forwards in time. About 100000 particles were released per day with locations weighted by an emission inventory such that each particle is associated with the same mass of CO

on release. North American emissions were based on the point, onroad, nonroad and area sources from the U. S. EPA National Emissions Inventory (area sources at 4 km resolution) plus Mexican emissions north of 24°N and all Canadian sources south of 52°N [*Frost et al.*, 2005]. The inventories are estimates for the year 1999. Outside this domain the EDGAR emission inventory was used [*Olivier et al.*, 1999]. Particles were carried for 20 days before removal from the simulation. The positions of these particles were recorded every 2 hours. The number of particles per unit volume gives an estimate of CO concentration away from the sources. FLEXPART was driven by forecasts and analyses of winds from the Global Forecast System model of NCEP (National Center for Environmental Prediction) at $1^\circ \times 1^\circ$ resolution on 26 pressure levels with a temporal resolution of 3 hours.

As described by *Stohl et al.* [2004], Lagrangian opportunities were sought by following these particles backwards in time from the operational areas of each aircraft (Pease, Faial and Creil) and recording whether (after $>$ 24 hours) the particles were in range of an aircraft. If the CO-tracer decrease backward in time was more than 20%, indicating influence of fresh emissions, the trajectory was excluded. Also, air masses were excluded if the RMS separation of particles (from their centroid) arriving in one tracer output cell ($1^\circ \times 1^\circ \times 1000$ m) exceeded 100 km plus 5% of travel distance. This eliminates cases with rapid back trajectory separation, indicating air being brought together from very different origins and therefore not a good candidate for a Lagrangian case study. The Lagrangian opportunities were ranked according to their CO-tracer mixing ratio weighted by the number of aircraft that could possibly sample it.

Once flights had taken place, particles were released from boxes of size $0.7^\circ \times 0.7^\circ \times 400$ m centered along the flight track and opportunities were ranked by measured CO.

Often the FLEXPART model with its Lagrangian opportunity criteria highlighted different targets to the UGAMP trajectory model with its emissions-tracer criteria, but on re-inspection the same targets were often identified by both models. Each group examined the forecast products that they were most familiar with: FLEXPART forecasts for the NOAA WP3-D team, the UGAMP RDF forecasts for the ITOP-UK team and both for the Falcon team. When agreement was spotted during discussion this lent weight to the decision to pursue a target. FLEXPART forecasts were focussed towards planning the upstream flights and were particularly useful in ruling out cases when dilution by mixing was predicted to be too great for the chemical contrast of the air mass to remain distinct.

Comparison was also important because the two Lagrangian models used forecast winds from different meteorological centres which could introduce differences in target locations of several hundred km on the European side of the Atlantic.

It will be shown in Section 5 that both models result in a similar quality of coincident matches, although there are many cases where only one of the models identifies a match due to the very strict, but differing, selection criteria. In the matching analysis FLEXPART was also driven by ECMWF analyses.

3. Airborne measurements

The instruments on the four aircraft participating in the Lagrangian 2K4 experiment and the characteristics of their measurements are summarised by *Fehsenfeld* [2006].

In order to infer changes in chemical composition following air masses, it was crucial to compare the measurements by the different aircraft flying in formation as close together as possible. Three comparison flights were made between the WP3-D and DC8 on 22 July, 31 July and 7 August. The DC8 and BAe146 made a rendezvous over the mid-Atlantic on 28 July. Two comparison flights were made between the BAe146 and Falcon: over England on 7 July and over France on 3 August.

The ozone comparison is of particular interest since it is used to indicate the net chemical transformation following air masses. For 22 July and 7 August, plotting WP3-D measurements on the x-axis against DC8 measurements on the y-axis shows high correlation (r^2=0.92, 0.99 with slopes of 1.01±0.01, 1.00±0.01) with the DC8 reading higher than the WP3-D by 0.1 and 2.5 ppbv averaged over the comparison period. On 31 July, ozone concentrations were low without much range but rapidly varying because one leg was close to the top of the boundary layer and the comparison indicated a poor slope (0.76±0.01) with DC8 reading lower than WP3-D by 1.5 ppbv. For 28 July, putting the BAe146 on the x-axis, there was high correlation with the DC8 (r^2=0.99) but a slope of 0.94 ± 0.01 because the DC8 reads higher at low concentrations (mean difference 0.6 ppbv). Finally, on 3 August, putting the Falcon measurements on the y-axis, there was a high correlation with the BAe146 (r^2=0.99) with the Falcon reading higher by 0.8 ppbv on average while on 7 July the Falcon read lower by 0.5 ppbv. Although there is clearly variation between comparisons using the same aircraft so that a systematic bias is difficult to estimate, these comparisons indicate a bias in ozone measurements moving across the Atlantic from the DC8 to BAe146 to Falcon of only 0.4 ± 2 ppbv.

For CO, the comparison was good between the DC8 and WP3-D. On 22 July, 31 July and 7 August r^2 was 0.99, 0.96 and 0.97 and in the mean the DC8 was offset from the WP3-D by +1.7, +3.5 and -0.6 ppbv. The comparison between the DC8 and BAe146 is hindered by the lack of data from the fast response LARC DACOM instrument on the DC8 on 28 July. However, whole air samples were analysed for CO by UCI. The comparison shows a large standard deviation as expected due to different sampling windows, but the DC8 also reads higher than the BAe146 by 7.5 ppbv. Plotting UCI CO data (on x-axis) against LARC CO for all flights of the DC8 during ICARTT, the slope is 0.96 with $r^2 = 0.98$. The comparison between the BAe146 and Falcon is also not as good as for ozone with the Falcon reading higher than the BAe146 by 2.5 ppbv on 7 July and 6 ppbv on 3 August. However, on 7 July concentrations varying between 250 ppbv and 75 ppbv were measured, associated with crossing North American fire plumes, so that the offset was less than 4% of the range.

Ambient air samples were circulated to the laboratories of the different groups associated with each aircraft. The hydrocarbon measurements were highly consistent [*Lewis*, 2006]. It was difficult to compare whole air samples from comparison flights due to the different sampling times and variability within the air masses. However, it is clear that the hydrocarbon fingerprints of samples taken within one air mass are very similar (typically using eqn.(2) $r > 0.9$).

The frequency of data recorded by instruments varies a great deal. Throughout this paper all data is shown with

10s resolution. Higher frequency data has been averaged over 10s windows centred on the time stamp. Lower frequency data (e.g., whole air samples) is repeated at every time-point throughout the sample interval. Data from all instruments on the DC8 and BAe146 aircraft was collated in this way into "data merges" for each flight.

4. The search for Lagrangian matches

4.1. Trajectory model matches

Trajectories were released at 10s intervals from flight tracks and integrated forwards and backwards so that all the associated "air masses" were followed over the same 35 day time interval (12UT 1 July 2004 - 5 August 2004). The four ICARTT-Lagrangian aircraft made 40 flights during the period of opportunity (6 July 2004 - 1 August 2004 plus the flights of the BAe146 and Falcon on 3 August), requiring 91901 trajectories from flight tracks. A time-point on a flight was labelled as a match if its associated trajectory shadowed a trajectory from another flight over the time window between the flights. If the flights were separated by less than 4 days, the comparison time window is extended to 4 days centred on the mid-time between the flights. The criteria for "shadowing" was taken to be a mean difference in latitude and equivalent potential temperature (θ_e) of less than 0.5° and 2K respectively, averaged over the trajectory time-window. For the comparison, θ_e was interpolated from the ECMWF analyses to points spaced at 6 hour intervals along the trajectories. Note that often the magnitude of change in (analysed) θ_e following a trajectory over the time-window is much greater than 2K (e.g., associated with mixing or radiative cooling) but a similar evolution must occur for both trajectories in a matching pair such that their average separation is less than 2K.

In principal the match criteria based on two variables alone could allow erroneous matches where a pair of trajectories followed the same history of latitude and θ_e but at different longitudes or altitudes. However, not a single case occurred out of the 4.1×10^9 trajectory pairs, indicating that there is negligable chance for trajectories to shadow each other this closely over a 4 day window unless they are within neighbouring air masses.

A single trajectory from flight-A may "match" with many trajectories from flight-B. Conversely, any one of those matching trajectories from flight-B may match with many other trajectories from flight-A ("converse matches"). The many-many relationship is complex, even if only one distinct air mass links the flights, because the two flights will have spent different times within the air mass and may have intersected it on several occasions. No trajectory from flight-A matches a trajectory from flight-B exactly. The complexity is reduced by selecting the "best" matching trajectory from flight-B for every time point along flight-A. The definition of best is also problematic. One could choose the match with the smallest latitudinal separation for example. However, this may select air masses that were sampled for a very brief time. The chosen method was to select the trajectory from flight-B that has the most converse matches with flight-A. In this way the "best match trajectories" are the most representative of a coherent ensemble of trajectories that match both flights. These trajectory-only (best) matches are marked by colour bars on the time series shown in Fig. 2a. Considering all ICARTT-Lagrangian flights there are 30887 best matching pairs.

4.2. FLEXPART model matches

CO-tracers were simulated by running the Lagrangian dispersion model FLEXPART forwards in time. The particles experience parameterized turbulence and convection, in addition to advection by the winds resolved in the ECMWF analyses. Their positions were stored every 2 hours. The flight tracks were divided into segments with intervals of 0.2 degrees from horizontal flight legs (or whenever the aircraft altitude changed by more than 50m below 300m, 150m below 1000m, 200m below 3000m or 400m above this). All particles located within 30km horizontally and 200m vertically of a segment were identified and traced forward for a maximum of 10.5 days. The centroid position of these particles and their standard deviation about the centroid was calculated. The North American CO-tracer was determined at all particle positions and averaged over those from each flight segment.

Matches were defined based on criteria, similar to those used for the identification of Lagrangian opportunities [*Stohl et al.*, 2004]: 1) the separation between Lagrangian samplings must exceed 12 hours and a distance of 800 km. 2) The CO-tracer mixing ratio must not decrease back in time by more than 20%. 3) The horizontal distance between the plume centroid trajectory and downwind measurement point plus the plume standard deviation must be less than 18% of the distance travelled. 4) The vertical separation between the plume centroid trajectory and a measurement plus the standard deviation must be less than 1000m plus 0.02% of the horizontal distance travelled.

In total, 395 FLEXPART "Lagrangian cases" were identified and ranked according to the distance criteria (3) and (4). By the time a plume has reached the mid-Atlantic these two criteria are generally less strict than the trajectory-match criteria (latitude separation $< 0.5°$ and θ_e separation < 2K). Some of these cases involved more than two aircraft flights and these were given greater weight in the ranking. In total there were 489 matches between flight time segments. These are marked by red triangles in Fig. 2a.

Although far fewer FLEXPART matches are depicted than trajectory matches, in Section 4.4 it will be shown that a similar number of coincident matches are pulled out by both models. This is because a much higher fraction of FLEXPART matches are coincident matches. Also many trajectory matches (up to 200) can be linked to one hydrocarbon match and only the best is indicated as the "coincident match".

4.3. Hydrocarbon fingerprinting

Multi-component hydrocarbon measurements provide a means for distinguishing air masses because their relative amounts are variable. In addition, photochemical ageing can be inferred from compounds with a range of different lifetimes with respect to OH reaction [e.g., *Jobson et al.* [1998]]. If a polluted air mass mixes with a clean background, containing almost zero hydrocarbon concentrations, then the ratio of any two hydrocarbons only evolves due to their different photochemical loss rates. Problems with comparing absolute concentrations from upwind and downwind samples of an air mass with variable concentrations, but distinct composition, are to some extent circumvented by considering ratios.

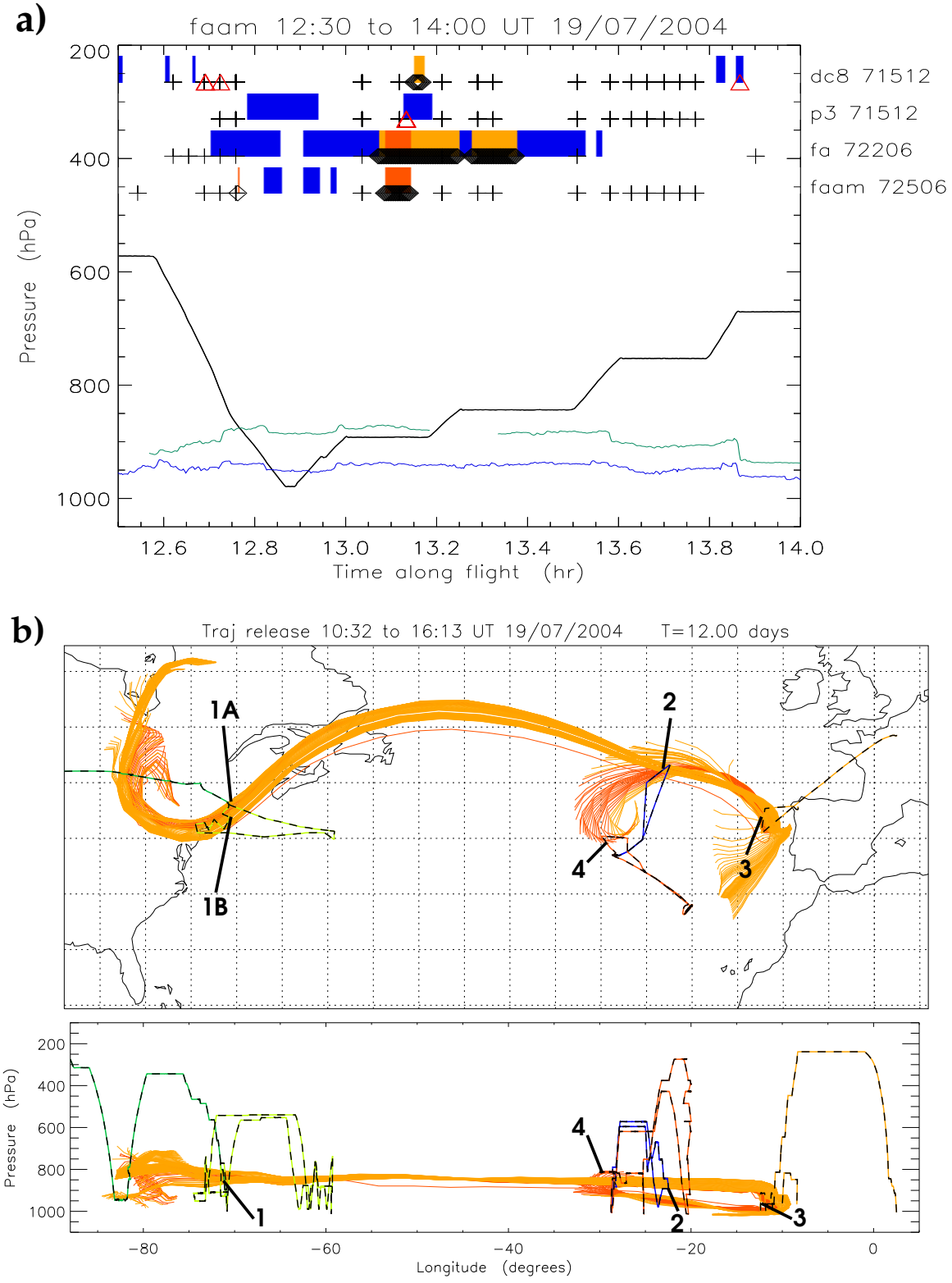

Figure 2. (a) Lagrangian matches shown versus time along the flight of the BAe146 aircraft on 19 July 2004. The black line shows pressure (hPa). The green and blue lines show CO and ozone using the y-axis (1000-C) where C is volume mixing ratio in ppbv. Matches are shown with four other flights: DC8 on 15 July, WP3-D on 15 July, Falcon on 22 July and BAe146 on 25 July. Crosses mark matching hydrocarbon samples. Blue colour bars indicate times with trajectory–only matches. Coincident matches are coloured and marked by diamonds. Red triangles mark FLEXPART matches. (b) Trajectories 6 days backwards and forwards from the flight track on 19 July (blue) that shadow trajectories from the other flights shown and also link air samples with similar hydrocarbon fingerprints ("coincident matches"). Matching flights are: DC8 15 July (dark green), WP3-D 15 July (light green), Falcon 22 July (orange) and BAe146 25 July (red). Lagrangian interceptions are numbered in time order.

Parrish [2006] examines the difficulties in using hydrocarbon ratios to infer age of air (since leaving the source region) that arise because air masses mix with others that are not clean and have different fingerprints because they have experienced different sources. The distribution of sources can be estimated using the footprint of a retroplume calculation using a Lagrangian dispersion model. It is typically found that when following a retroplume backwards in time it spreads slowly until close to the boundary layer. Here, it will be assumed that the upwind measurements are taken above the boundary layer and that little mixing occurs before the downwind measurements. Under these assumptions, upwind and downwind air samples can be described as having the same composition if their fingerprints of hydrocarbon ratios match, after accounting for the evolution associated with OH loss. *Arnold et al.* [2006] also examine the effects of assuming different backgrounds, estimated from the observations, and attempt to infer the mixing rate averaged along trajectories in addition to the OH concentration.

Hydrocarbon fingerprints were compared between all pairs of "whole air samples" (WAS-pairs) collected by the four aircraft. Matches were identified in the following way.

1. The concentration ratio, h_i, of 8 hydrocarbons to ethane is found for upwind and downwind flights (to factor out dilution by mixing to a clean background). The hydrocarbons used in order of increasing reactivity with OH are: acetylene, propane, benzene, iso-butane, pentane, hexane, ethene and propene ($i = 1, .., 8$).

2. The upwind ratios are adjusted to account for photochemical loss between measurement times by taking logs and using the rate coefficients for OH reaction, k_i, assuming a constant OH concentration:

$$y_i = \ln(h_i(t_1)) - (k_i - k_{ethane})[OH](t_2 - t_1) \qquad (1)$$

where t_1 and t_2 are the upwind and downwind sample times, and y_i is described as the "adjusted upwind ratio". Note that the ethene and propene concentrations were not adjusted for OH reaction before calculating their ratios. As discussed in Section 6.2, their ratios are not observed to decrease rapidly, as would occur from OH loss, which may point to secondary production from other hydrocarbons.

3. For each WAS-pair the scatter plot of downwind and adjusted-upwind ratios is compared with the 1:1 line and closeness of fit measured with the statistic:

$$r = 1 - \frac{\sqrt{\frac{1}{N-1}\sum \frac{1}{2}(y_i - x_i)^2}}{X} \qquad (2)$$

where $x_i = \ln(h_i(t_2))$ and $X = \max\frac{1}{2}(x_i+y_i) - \min\frac{1}{2}(x_i+y_i)$ is the range of values for that match. Note that the closest point on $x = y$ to a measurement-pair (x_i, y_i) is $x = y = \frac{1}{2}(x_i + y_i)$ separated by the distance-squared $\frac{1}{2}(y_i - x_i)^2$. Therefore, the quantity $1-r$ equals the RMS deviation from the line $x = y$ divided by the range in the data. N is the number of hydrocarbons (in addition to ethane) measured in common on both flights (cases where $N < 4$ were rejected).

4. The pair is labelled a "WAS-match" if r exceeds the 90th percentile obtained using all WAS-pairs from that pair of aircraft. The r-threshold is allowed to vary between pairs of aircraft because there are far fewer good (high-r) matches between aircraft separated by long times. The hydrocarbon matching criterion is therefore very strict considering WAS-pairs collected by the DC8 and WP3-D close to the emissions from the USA, and relaxed for matches involving the BAe146 and Falcon flying several days downwind.

5. The matching procedure was repeated for varying OH to find the concentration that gave the highest value for r at the 50th and 90th percentiles. This "optimum" OH concentration of 1×10^6 molec cm^{-3} was used to define WAS-matches. It is consistent with global estimates by *Prinn et al.* [1995]. It was found that the identification of Lagrangian matches is quite insensitive to variations in OH in the range 0 to 2×10^6 molec cm^{-3} because the longest lived compounds are barely affected by the OH-adjustment. The trans-Atlantic matches are most sensitive due to the long time elapsed between samples. *Arnold et al.* [2006] investigate the OH concentration required to optimise matches in each Lagrangian case when also allowing for mixing.

In total there are 224796 matches meeting the fingerprint criteria. However, most of the WAS-matches between samples collected by the DC8 and the WP3-D are not linked by trajectories but simply reflect the degree of similarity between air masses over the East Coast USA, close to the emissions. When DC8-DC8, P3-P3 and DC8-P3 matches are excluded, the number of matches reduces to 46834. WAS-matches are marked by crosses on the time series in Fig. 2a.

4.4. Coincident matches

A search was made for the subset of all match-trajectories that link both time-segments associated with a WAS-pair. Every WAS measurement was associated with a 6 minute time-segment in searching for linking trajectories. Samples typically take less than a minute to fill but the window was extended to allow for phase errors in the matching trajectories. These "coincident matches" are marked by the diamonds and a colour bar on Fig. 2a. The colour corresponds with the colour of the matching flight track shown in Fig. 2b.

All the "coincident match" trajectories from the BAe146 flight track (dark blue) on 19 July are shown in Fig. 2b extending 6 days backwards and 6 days forwards. The coincident trajectories' colours correspond with the last flight that they intersect.

Using all 40 ICARTT-Lagrangian flights, only 545 WAS-matches were also linked by matching trajectories. Since the trajectories are released every 10s from the flight tracks, there are typically many matching trajectories associated with each of these cases. These will be called "coincident-match trajectories": 8275 were found between all ICARTT flights, reducing to 1141 coincident matches when those between the USA aircraft are excluded (DC8-DC8, P3-P3, DC8-P3).

A similar search was made for all FLEXPART-matches that link with both ends of a WAS-match (called FH-linked for FLEXPART-Hydrocarbon). The time-segments centred on the time-stamp for WAS samples and FLEXPART matches were given a width of 6 minutes and the flights were divided into 10s intervals (just as for the trajectories) for the purposes of these searches. 1947 FH-linked matches were found between all ICARTT flights, reducing to 453 FH-linked matches when those between the USA aircraft are excluded (DC8-DC8, P3-P3, DC8-P3).

Finally, consistency between the two models and WAS-matches is investigated by searching for coincident-match trajectories that link with both time-segments of each FLEXPART-match (called CF-linked for coincident-FLEXPART). All the matches and corresponding time-stamps are listed at *http://www.met.rdg.ac.uk/∼swrmethn/icartt*. Only the best five Lagrangian cases will be discussed in Section 6.

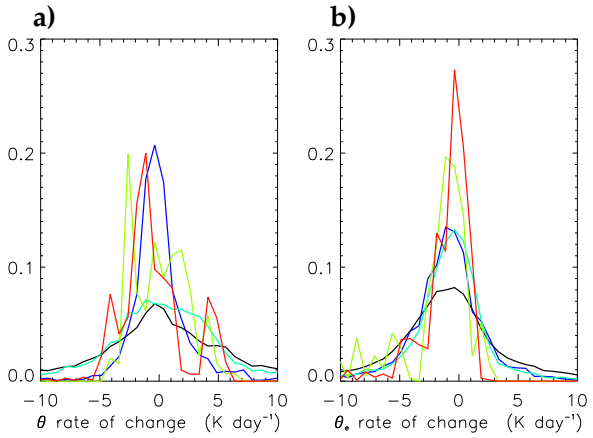

Figure 3. Normalised histograms showing average rate of change along match-trajectories between upwind and downwind observations for (a) potential temperature and (b) equivalent potential temperature. The curves show results for different types of matches: coincident trajectory-hydrocarbon (red), FLEXPART-hydrocarbon (green), trajectory-only (blue), hydrocarbons-only (cyan) and random pairs of time-points from matching flights (black). The bin size used was 0.75 K day^{-1} and the sum over bins equals one for each histogram.

5. Evaluation of matches using independent tracer observations

The quality of the independent model and hydrocarbon matches and their coincident matches is assessed using further independent datasets: measurements of temperature, humidity, CO and ozone. A running median filter with a time-window of 6 minutes was passed through all the time series of aircraft data. A running median was used (rather than running mean) because it preserves the location and gradient associated with boundaries between distinct air masses, while removing rapid fluctuations that cannot be associated with particular trajectory behaviour. It has little impact on the time series far from emissions, but smooths out rapid fluctuations over the USA close to sources, especially in the boundary layer. The filtered aircraft data is interpolated to the release points used for the trajectories (at 10s intervals). Differences between upwind and downwind potential temperature (θ), equivalent potential temperature (θ_e), CO and ozone are calculated for every match. PDFs of these differences are plotted for the various methods: trajectory-matches, WAS-matches, coincident-matches and FH-linked matches.

The potential temperature difference between downwind and upwind samples is divided by their time separation to give the average rate of change following air masses. The resulting PDF (Fig. 3a) is strongly peaked on slow cooling (-1 to -2 K day^{-1}) for coincident trajectory-hydrocarbon matches and a similar PDF is obtained using FLEXPART-hydrocarbon (FH-linked) matches. This value is consistent with constant radiative cooling under clear skies. The trajectory-only matches are also strongly peaked near zero, indicating that most of the trajectories that match are almost isentropic. In contrast, the PDF for WAS-matches is much flatter indicating that many samples with similar hydrocarbon fingerprints are not within the same air mass (i.e., linked by trajectories).

Note that the black curve was obtained by selecting n time-points at random from the time-series of two flights and using observed θ from these pairs of points to calculate $(\theta_2 - \theta_1)/(t_2 - t_1)$. Each pair of flights was weighted by setting n equal to the number of trajectory matches between them. The "random" histogram illustrates the similarity of the air masses sampled on flights that are linked, irrespective of Lagrangian connections. Therefore, its values cannot be interpreted as heating rates following air masses. The identification of Lagrangian matches is only successful if the PDF for matches is more strongly peaked than the PDF for randomly selected time-points. Clearly, WAS-matches alone are not significantly different from random selection.

Note that the coincident and FH-linked PDFs have a secondary peak at a heating rate of about 5 K day^{-1}. This can be attributed to the time-averaged rate of latent heat release in ascending air masses experiencing condensation. A better thermodynamic tracer of air masses is equivalent potential temperature, θ_e, that is conserved for the pseudo-adiabatic process of a saturated air mass experiencing condensation. The PDFs for rate of change of θ_e (Fig. 3b) are even more strongly peaked on weak cooling for coincident and FH-linked matches. However, the coincident-match histogram also shows a peak at a cooling rate of -5 K day^{-1}. All matches contributing to this peak are associated with air masses travelling partly within the marine boundary layer over the cool ocean surface while looping polewards in Lagrangian Case 3 (Section 6.1). The FH-linked PDF shows a secondary peak for heating, but this appears to be spurious and associated with cases where the trajectory-match criteria would fail. Trajectory-only matches are clearly not as good as coincident matches. θ_e reveals that although trajectory-matches may occur in the same isentropic layer (range of θ values) they can have the wrong specific humidity for a Lagrangian match. The additional requirement for a hydrocarbon match pulls out the matches with similar humidity. Conversely, the PDF for WAS-matches is more peaked for θ_e than for θ. This shows that the θ_e signature and hydrocarbon fingerprint are correlated, both being indicative of air mass origin, even if two samples are not linked by trajectories.

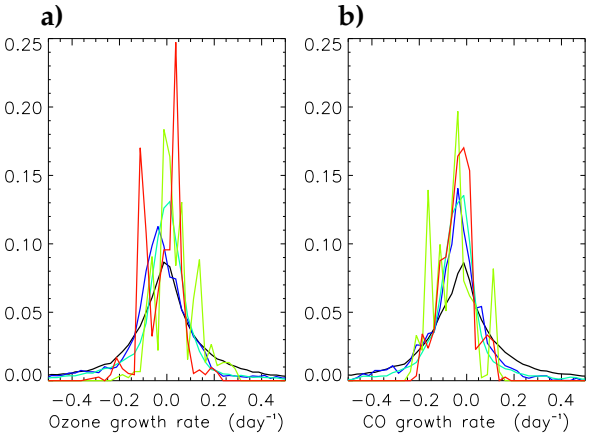

Figure 4. Normalised histograms showing average growth rate along match-trajectories between upwind and downwind observations for (a) ozone and (b) carbon monoxide. Lines coloured as in Fig. 3. The bin size is 0.025 day^{-1}.

Upwind and downwind matching observations are used to estimate "growth rates" for Fig. 4 using:

$$\sigma_c = \frac{1}{t_2 - t_1} (\ln C_2 - \ln C_1) \quad (3)$$

In the case of a tracer with a photochemical lifetime much longer than the mixing timescale, such as CO, mixing is expected to dominate changes following an air mass. Mixing with a uniform dilute "background" would result in exponential decay of concentration with timescale $-1/\sigma_c$. However, typically pollution plumes do not have much higher CO concentrations than their surroundings, since CO is rather long-lived, and dilution of CO within the centre of the plume will be slow even if turbulent mixing is active since the CO-gradients will be weak. In this case, $-1/\sigma_c$ cannot be interpreted as a turbulent mixing timescale. The narrow PDF peak for "CO growth rate" occurs between -0.05 and -0.10 day^{-1}, indicative of a slow dilution timescale of 10-20 days. Weak CO increase is inferred from some match-pairs. This is most likely to result from a slight mismatch in a plume with high variability. For example the downwind flight may have crossed the maximum plume concentration while the upwind aircraft may have sampled only the flanks or flown just above or below the air mass sampled downstream.

Comment: why is O3 chemistry slow - it is not always slow - the NET change due to photochemistry can be small but the individual terms can still be large. Also, what about mixing - this can affect O3 as well as CO.

The "ozone growth rate" PDF for coincident matches is bimodal with two strong peaks either side of zero, consistent with slow photochemistry and mixing. The positive peak is perhaps attributable to net photochemical ozone production in the polluted Lagrangian matches, although positive and negative peaks could arise through mixing and on balance there is little ozone change. The FLEXPART model matches do not exhibit bimodality, picking out fewer cases with ozone decrease. This is consistent with the FLEXPART match identification criteria which exclude clean air cases with North American CO tracer below 50 ppbv. Stronger decrease and increase is seen for a few matches. Photochemical modelling effort to explain the observations will be focussed on the best Lagrangian cases described in the next section.

6. The best ICARTT-Lagrangian cases

Overall, the matching methods agree that there were five main Lagrangian-cases linking three flights or more across the Atlantic, although coincident and FLEXPART matches sometimes have slight timing differences.

6.1. Air mass trajectories and intercepting flights

6.1.1. Case 1: USA to Portugal.

Figure 2b shows the trajectories for all coincident matches with the BAe146 flight on 19 July 2004. The orange trajectories link with the Falcon on 22 July off the coast of Portugal and some of them also link with the DC8 as it descended into Pease on 15 July. The red trajectories also link with the BAe146 on 25 July as the air returned towards the Azores from close to Portugal.

Examination of coincident matches along the Falcon flight track (not shown) reveal two distinct cases. Coincident matches with the BAe146 on 19 July occur on a level run at 913 hPa off the Portuguese coast. Matches with the BAe146 on 25 July only occur on a lower level run (at 965 hPa) within the marine boundary layer (red trajectories). Similarly, coincident matches along the DC8 track on 15 July occur with the BAe146 19 July at higher altitude (855 hPa) than with BAe146 25 July (902 hPa). Therefore, this case has been split into two, with case 1B occurring at slightly lower altitude than case 1A. Both sets of trajectories descend slightly across the Atlantic under clear skies. The split is confirmed by the distinct hydrocarbon fingerprints for the two cases. Case 1B is more polluted and has a higher butane/ethane ratio.

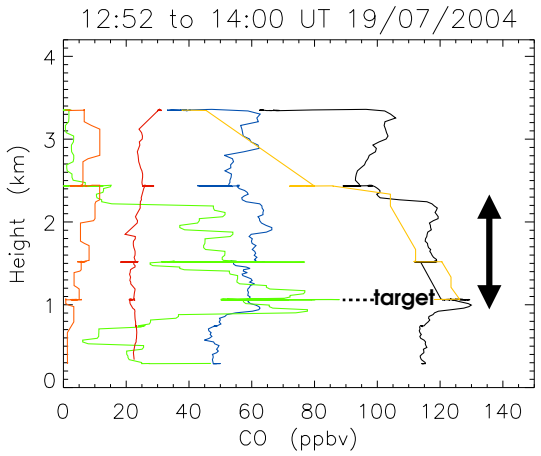

Figure 5. Profiles of measurements made by the BAe146 between 12:52 and 14:00 UT on 19 July 2004. Black, CO (ppbv). Blue, ozone (ppbv). Green, sulfate aerosol ($0.1\times\mu$g m$^{-3}_{\rm STP}$). Yellow, ethane ($0.01\times$ ppbv). Orange, PAN ($0.01\times$ ppbv). Red, $\theta_e - 300$ (K). The y-axis uses the pressure-height coordinate $z = 44330.77[1 - (p/p_0)^{0.19026}]$m where $p_0 = 1013.25$ hPa.

Both the orange and red trajectories shadow trajectories from the WP3-D flight on 15 July (close to point B on Fig. 1) but due to a system malfunction no WAS measurements were made on this half of the flight and therefore hydrocarbon fingerprints cannot be compared. However, the match with the WP3-D is also indicated by the FLEXPART model (red triangle in Fig. 2a).

Figure 5 shows measurements made by the BAe146 in ascent through the polluted layer. The highest CO, ethane and sulfate aerosol concentrations occur at the target level (1.05 km or about 900 hPa in Fig. 2a) that matches the other four flights. The aerosol shows most contrast with the cleaner layer above and the marine boundary layer. The polluted layer extends from 0.9 km to 2.3 km. Equivalent potential temperature (θ_e) hardly varies with altitude even though there is marked layering in composition, especially in aerosol. This accords with the trajectories which indicate that the entire column from the ground to 2.3 km shares a similar geographical origin. Within the marine boundary layer, turbulent mixing enables contact with the ocean surface contributing to higher humidity and ozone loss (photochemically and through deposition). Ozone is seen to be lower in the marine boundary layer, although still well elevated compared to clean episodes near the Azores in the same month ($[O_3] \sim 10-20$ ppbv – see *Lewis* [2006]). There is a rapid increase in concentrations at 0.9 km, indicating

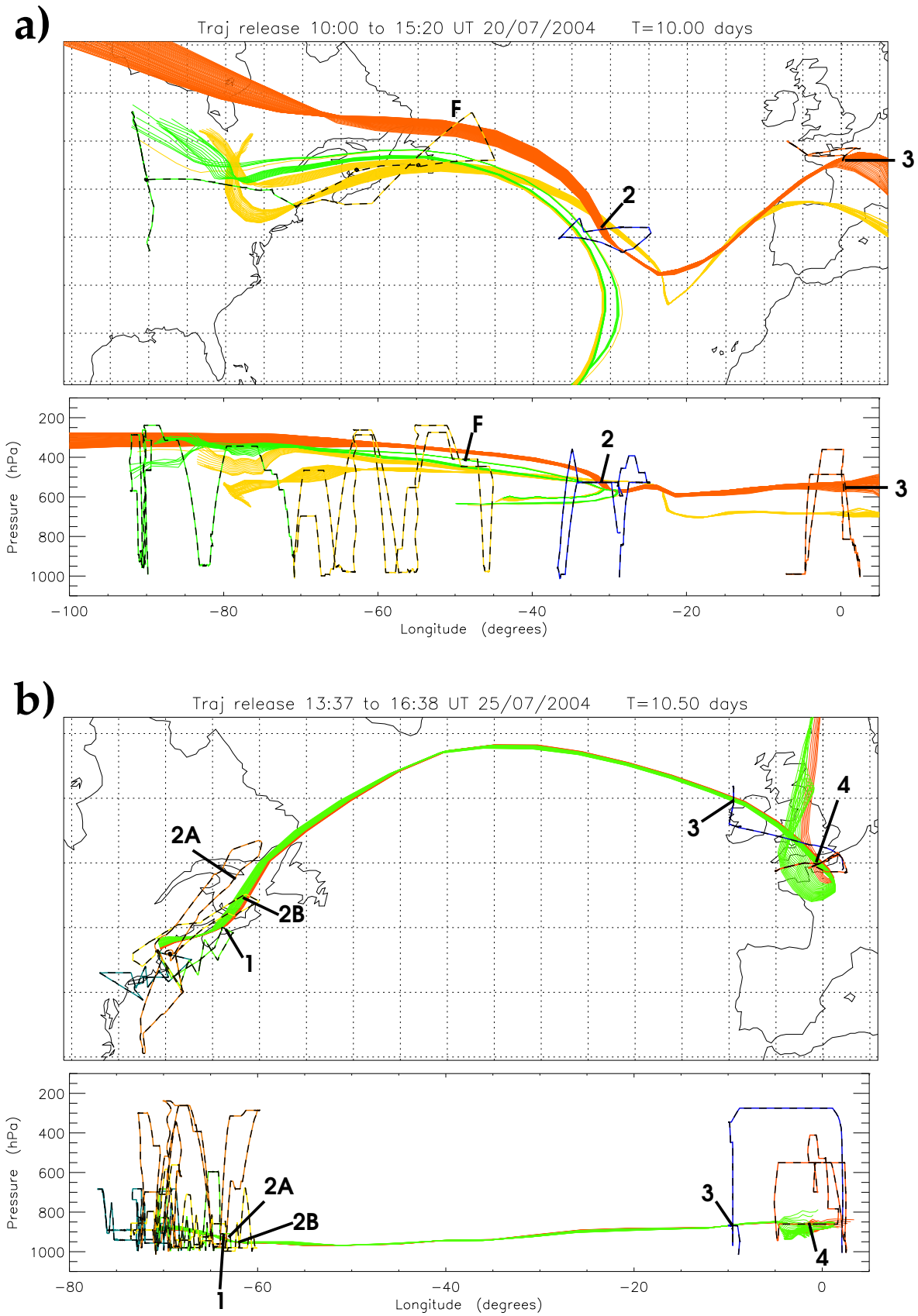

Figure 6. Lagrangian links between hydrocarbon samples from different flights with similar fingerprints ("coincident matches"). (a) **Case 2**: trajectories 5 days forwards and backwards from the BAe146 flight track on 20 July (blue). Matching flights are DC8 15 July (green), DC8 18 July (yellow) and Falcon 23 July (red). F marks the intersection of the Alaskan fire plume by the DC8 on 18 July. (b) **Case 3**: trajectories 5.25 days forwards and backwards from the Falcon flight track on 25 July (blue). Matching flights are WP3-D 20 July (dark green), WP3-D 21 July (light green), WP3-D 22 July (yellow), DC8 22 July (orange) and Falcon 26 July (red), labelled in time order.

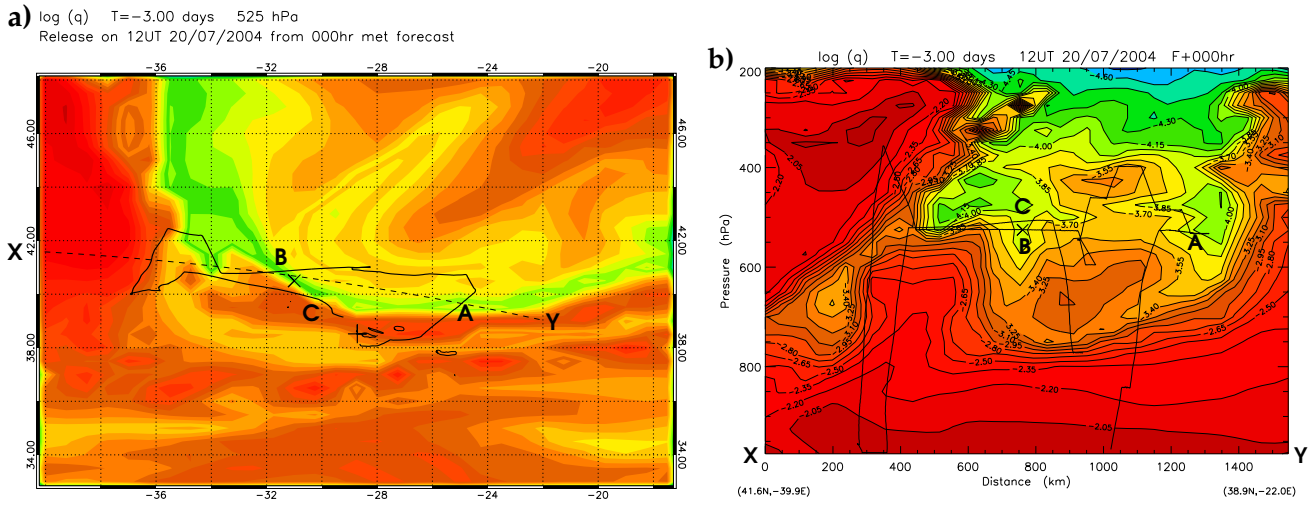

Figure 7. (a) RDF3D reconstruction of specific humidity ($\ln q$) on the 525 hPa surface, 12UT 20 July 2004. The flight track of the BAe146 is shown shifted relative to air mass locations at 12 UT. At this level the aircraft intercepted an Alaskan fire plume at points A, B and C. The plume is co-located with a narrow filament of dry air (green). The + symbol marks Faial. Longitude and latitude are labelled around the map. (b) Great circle cross-section XY, marked by the dashed line in (a). The BAe146 flight track is projected onto the section.

that mixing is weak above the boundary layer and that this layer has not been in contact with the ocean. Weak mixing would be consistent with the slow decrease in CO (see Table 1).

The extremely high level of sulfate aerosol was also observed off the East Coast USA in the lower troposphere and on several other days in the Azores region (BAe146 flights on 17, 20, 22 July). Source contributions estimated using FLEXPART in retroplume mode indicate that this originates from the coal burning power plants, especially in the Ohio River Valley and picks up further emissions approaching the East Coast USA. The scenario of pollution leaving the continental boundary layer and then forming two layers over the ocean, within and above the marine boundary layer, was also observed during the third Lagrangian case in ACE-2 [*Johnson et al.*, 2000], although for pollution leaving Western Europe. In that case the aerosol size spectrum and composition did not evolve significantly over the 30 hour window of observation.

6.1.2. Case 2: Alaskan fire plume.

Throughout July 2004, the mid to upper troposphere above North America and the Atlantic was highly perturbed by emissions from boreal forest fires in Alaska and later in Canada [*Pfister et al.*, 2005]. High CO levels were observed throughout much of the Northern Hemisphere towards the end of the month. A number of Lagrangian links were made between flights sampling these fire plumes, even though the emissions and tracer perturbations were not included in the Lagrangian model forecasts. Some links were fortuitous, but the best occurred when the extremely concentrated plumes were noted by the upstream aircraft and then forward trajectories from those tracks were used to predict the subsequent path of the air. Case 2 is the best linked of these matches and occurred after the DC8 had sampled an intense plume near Newfoundland on 18 July (point F in Fig. 6a).

Figure 7a shows the flight track of the BAe146 relative to the plume on 20 July. Since air can travel 100s of km while a flight is occurring, the track coordinates have been shifted using short forward and backward trajectories to the estimated positions of sampled air masses at an instant, 12UT. This enables clearer comparison of the flight track with the air mass structure simulated for a single time frame using the Reverse Domain Filling trajectory technique for a 3D domain (RDF3D) [*Methven et al.*, 2003]. Back trajectories were released from the 3D grid over the Azores region. The specific humidity, q, from the ECMWF analyses was interpolated to the origin of every trajectory (3 days before "arrival" on the grid) and $\ln q$ was used to colour their arrival points. The driest air (green) was strung out in a long, thin filament at the 525 hPa level, and contained the fire plume. This plume was intercepted four times: near points A, B, C and in the descent home after C.

Figure 7b shows the specific humidity structure on cross–section XY. The fire plume occurred within dry intrusions

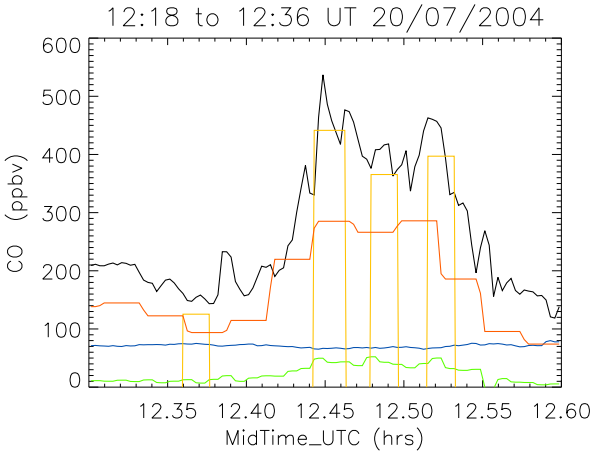

Figure 8. Time series of measurements made by the BAe146 through fire plume B between 12:18 and 12:36 UT on 20 July 2004. Black, CO (ppbv). Blue, ozone (ppbv). Green, organic aerosol ($0.1\times\mu$g m^{-3}_{STP}). Yellow, ethane ($0.01\times$ ppbv). Orange, PAN ($0.01\times$ ppbv).

that had descended from close to tropopause level over North America – presumably the level that material was carried to by convection above the fires.

The best trajectory match with the DC8 flight track is at point A, but unfortunately hydrocarbon samples were not measured there. However, back trajectories from point B pass just above the flight level of the DC8 through the plume at point F in Fig. 6a (just failing the θ_e trajectory match criterion). Three WAS measurements were made within plume B as seen for ethane on Fig. 8 and these had a very high correlation with the three WAS measurements by the DC8 within the plume. CO, PAN and organic aerosol were extremely elevated within the plume, while sulfate aerosol was almost negligable.

Interestingly, ozone concentrations are slightly lower within the plume than its surroundings. However, the downwind minus upwind observations (Table 1) and Lagrangian photochemistry models (the Master Chemical Mechanism and CiTTyCAT) indicate that ozone increased between the two flights [*Whalley et al.* [2006]; *Real et al.* [2006]]. The low ozone is therefore a puzzle. It may arise because the air that is carried up with pollution from the fires starts with very low ozone concentrations relative to typical values just below the tropopause. Additionally, pollutant levels may be so high immediately downwind of the fires that photochemical ozone loss occurs.

6.1.3. Case 3: USA to Ireland.

Another excellent example of pollutant export across the Atlantic at low levels occurred after a period of slack winds and pollutant build up over East Coast USA. The WP3-D aircraft deliberately sampled air downwind of the New York urban area on 20 July and then targetted the same air on two successive days as it slowly crossed the Gulf of Maine and Nova Scotia. The DC8 also intercepted this air during its flights on 20 and 22 July. As shown in Fig. 6b, the Falcon flew from France to intercept the air mass just west of Ireland on 25 July. The best Lagrangian links occurred quite close to the Global Atmospheric Watch observatory at Mace Head on the outbound flight of the Falcon, rather than its return flight to France (a few hours later). Note that the FLEXPART matches were indicated at about 850 hPa on the initial descent of the Falcon to low levels off the Irish coast (15:42UT). There are also trajectory matches at this time but no hydrocarbon sample was taken. The coincident trajectory-hydrocarbon matches occur on the level run at 870 hPa in the window 15:55-16:01 UT centred on the matching hydrocarbon sample. CO and ozone levels are very similar for these two flight segments, indicating that the matches are in essentially the same air mass. Finally, the target was forecast to cross Ireland and SW England overnight and the Falcon again attempted to intercept it over the English Channel on 26 July.

Note that there were many coincident matches between the three WP3-D flights with trajectories that subsequently passed far to the north of Ireland, spread between Greenland and the Norwegian Sea. Smart balloons were also released into the pollution plume and followed it across the Gulf of Maine [*Riddle et al.*, 2006]. The highest concentrations were oberved below and to the south of the matches with the Falcon.

6.1.4. Case 4: Upper level export by frontal system.

On 27 and 28 July a cold front progressed slowly eastwards across the East Coast USA. Pollution that had been building up during the preceeding week was exported in upper level and lower level flow. *Cooper* [2006] presents a detailed case study. Trajectories following the winds resolved by ECMWF analyses show ascent in a warm conveyor belt (WCB) from SE USA along the East Coast to the upper troposphere near Nova Scotia. There was also much deep convection over the eastern USA which would have carried pollutants into the upper troposphere where it could then be advected in the strong westerlies across the Atlantic.

The aim of the ICARTT-Lagrangian experiment was to sample air masses after rapid contact with surface emissions had ceased and then again downwind. Therefore, cases strongly influenced by convection or boundary layer mixing are not analysed here. The FLEXPART model indicated a Lagrangian match between the mid-troposphere over the USA sampled by the WP3-D on 27 July (marked "2" in Fig. 9a) and the upper troposphere to the west of the Azores

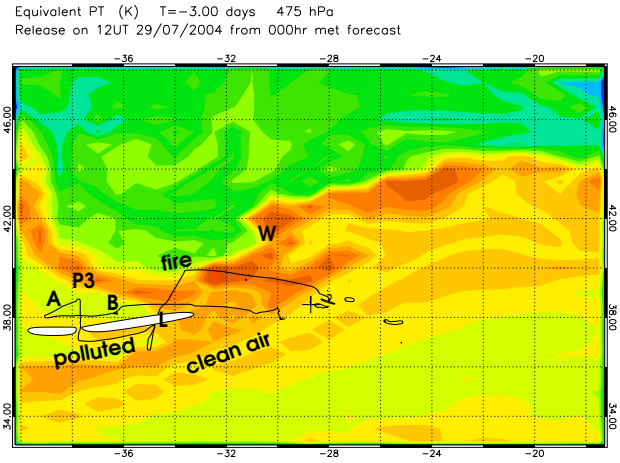

Figure 9. RDF3D reconstruction of θ_e on the 475 hPa surface, 12UT 29 July 2004. The flight track of the BAe146 is shown shifted relative to air mass locations at 12 UT. A long line of deep convection (marked in white) was first crossed at point L. Data on the descent from A to B is shown in Fig. 11. The descent was in polluted air, while models indicate that the air south of the front (yellow) was clean. W marks a weak frontal wave.

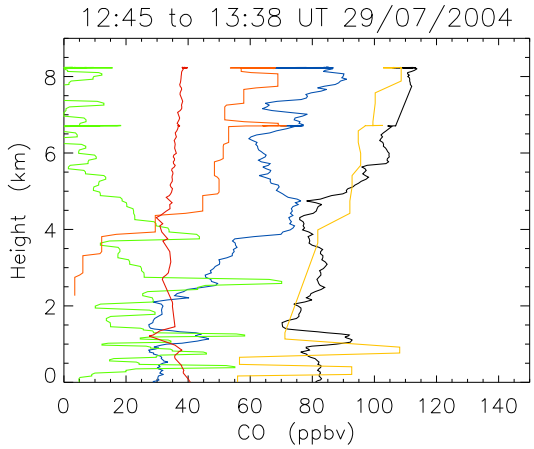

Figure 10. Measurements on descent through WCB outflow made by the BAe146 between 12:45 and 13:38 UT on 29 July 2004. Black, CO (ppbv). Blue, ozone (ppbv). Green, sulfate aerosol ($0.01\times\mu$g m$^{-3}_{\rm STP}$). Yellow, ethane ($0.01\times$ ppbv). Orange, PAN ($0.01\times$ ppbv). Red, $\theta_e - 300$ (K).

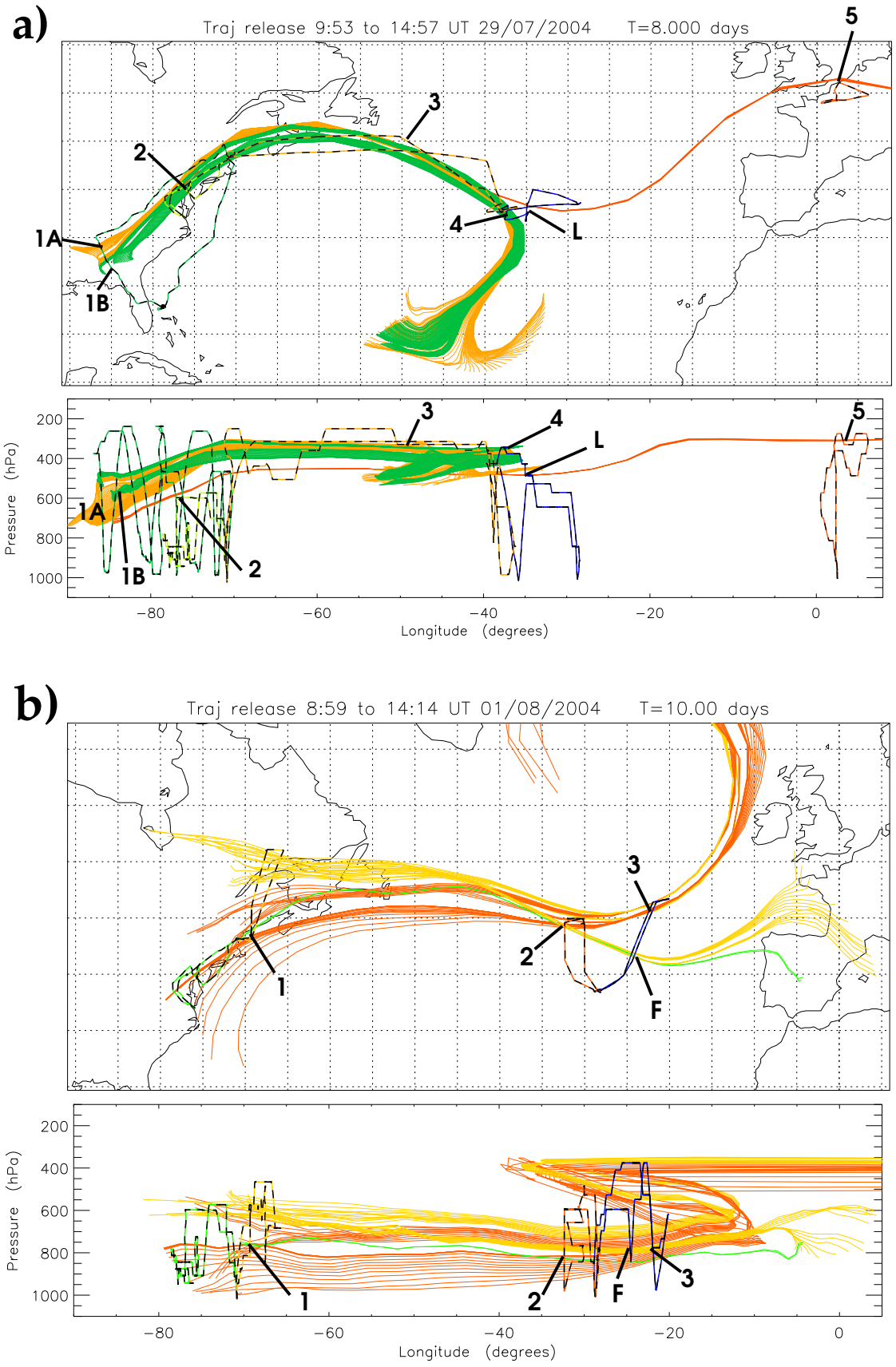

Figure 11. Lagrangian links between hydrocarbon samples from different flights with similar fingerprints ("coincident matches"). (a) **Case 4**: trajectories 4 days forwards and backwards from the BAe146 flight track on 29 July (blue). Matching flights are DC8 25 July (dark green), WP3-D 27 July (light green), DC8 28 July (orange) and Falcon 31 July (red), labelled in time order. L marks location of line convection. (b) **Case 5**: trajectories 5 days forwards and backwards from the BAe146 flight track on 1 August (blue). Matching flights are WP3-D 27 July (green), WP3-D 28 July (yellow), BAe146 31 July (red). F marks interception of a fire plume.

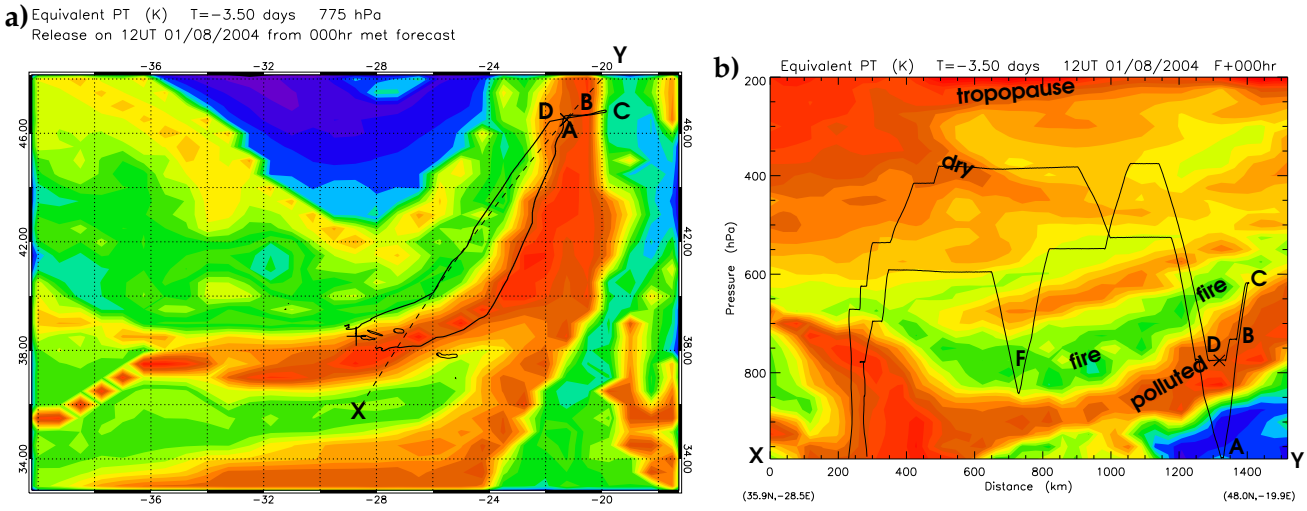

Figure 12. (a) RDF3D reconstruction of θ_e on the 775 hPa surface, 12UT 1 August 2004. The flight track of the BAe146 is shown shifted relative to air mass locations at 12 UT. A run was made at this level through the front between points B and D. The + symbol marks Faial. (b) Great circle cross-section XY. The BAe146 flight track is projected onto the section. The cross at point D marks the Case 5 Lagrangian match in the polluted air just above the θ_e maximum. Point F is a Lagrangian match with the WP3-D in a forest fire plume.

sampled by the BAe146 on 29 July. The location of this air mass, as modelled by FLEXPART and the UGAMP trajectory model, is marked "P3" on Fig. 10. Clearly, it is displaced to the north relative to the BAe146 flight track and just fails the trajectory-match criterion. However, tracer concentrations were observed to be horizontally uniform in this area, probably due to mixing over the USA, making a reasonable Lagrangian match between the WP3-D and BAe146. Also, their hydrocarbon fingerprints were highly correlated.

The BAe146 also has coincident matches with the DC8 on 25 and 28 July and Falcon on 31 July. On the outbound track of the BAe146 (see Fig. 10), a fire plume was encountered in the cold, dry air (low θ_e) at the northernmost point before turning south into the warm conveyor belt outflow. A long line of deep convection was crossed. It was observed on the aircraft navigation radar to extend at least 100 km to the east and west, although only 10 km wide with cloud tops at around 270 hPa. The best Lagrangian match with the Falcon on 31 July (red trajectories in Fig. 9a) is with air close to this line of convection (below the main pollution). It was not possible to return across the line convection immediately due to the extreme updraft velocities and was followed for about 200 km to the west, climbing upwards in steps before crossing northwards through a break at FL270 (about 8.1 km). Permission was not granted by air traffic control to climb higher although pollutant levels were clearly increasing with height. The best coincident matches with the DC8 on 25 and 28 July were south of the line convection on the highest flight level (Case 4A in Table 1 shown by orange trajectories in Fig. 9a) but north of the line convection with there are also coincident matches with the DC8 on 25 July (Case 4B in Table 1 shown by green trajectories).

Figure 11 shows the descent through the WCB from the highest flight level at point A (matching hydrocarbon fingerprint with the DC8 and WP3-D) to 1000 feet above the sea at point B. The polluted outflow layer is seen above 5 km where hydrocarbon concentrations increase with height. This layer was convectively stable ($\partial\theta_e/\partial z > 0$), enabling the persistence of layering in constituents. PAN is much higher than in the low level export Case 1, although about five times lower than in the Alaskan fire plume Case 2. PAN is correlated with ozone above 5 km. Sulfate aerosol concentrations are much lower than in Case 1 (note the units for aerosol have been divided by 10). This may be a signature of the contrast in origin with Case 1 (SE USA rather than NE) and/or the influence of wash out on sulfate in the warm conveyor belt.

Below the WCB outflow the atmosphere was close to saturation and convectively neutral (θ_e approximately constant). From 1.0 to 1.3 km there is a dry layer of high CO, ozone and

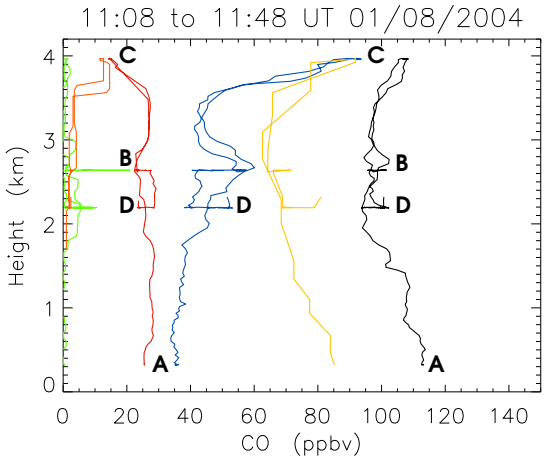

Figure 13. Measurements on ascent and descent across frontal surface made by the BAe146 between 11:08 and 11:48 UT on 1 August 2004. Black, CO (ppbv). Blue, ozone (ppbv). Green, sulfate aerosol ($0.1\times\mu$g m^{-3}_{STP}). Yellow, ethane ($0.01\times$ ppbv). Orange, PAN ($0.01\times$ ppbv). Red, $\theta_e - 300$ (K). Points A, B, C and D along the track are marked. The Case 5 Lagrangian match is on the level run to point D.

sulfate aerosol. Within the boundary layer below there are two prominent spikes in sulfate and ethane. Given the mid-ocean location, it seems likely that these were ship plumes. Back trajectories from the profile below 1.3 km indicate that this air was confined within the Azores High over the Atlantic between 20 and 40N for at least 20 days.

6.1.5. Case 5: Low level export by frontal system. The air from the polluted boundary layer over the USA that did not fall within the footprint of the WCB or get lofted by convection was exported to the east by the slower winds in the lower troposphere. Warm, moist air with high θ_e from the SE USA was advected along the East Coast ahead of the surface cold front picking up pollution and then out towards the Azores (red trajectories in Fig. 9b). Air with parallel trajectories just to the east passed only over the ocean and did not pick up pollution. The front passed over the Azores on 1 August 2004 and the warm sector (high θ_e) can be seen at 775 hPa in Fig. 12a. Air on the northwestern flank of the θ_e maximum was polluted while air on the southeastern flank was cleaner due to its trajectories missing landfall over the USA. The front was forward sloping (tilts up towards the south and east), usually indicative that frontogenesis has stopped (Fig. 12b). Mixing across the frontal surface reduced the contrast between these air masses.

The best Lagrangian matches occurred on the polluted northwest side of the front on descent towards A, at point B on ascent and descent and then a level run to D (see Fig. 12b). It can be linked to the BAe146 intersecting the front on 31 July and the WP3-D on 28 July. Trajectory-matches with the WP3-D on 27 July and DC8 on 25 July are more tenuous Lagrangian links because the low level export is likely to have been modified by mixing of emissions from the continental boundary layer before crossing the coastline.

Figure 13 shows measurements on ascent and descent across frontal surface between points A and D. The polluted side of the front was crossed on ascent through B, descent to B and then on a slightly lower level run to D. At these locations CO and ethane are elevated relative to their surroundings, but not a great deal. Sulfate aerosol shows greater contrast with the clean side of the front, although is clearly much lower than in Case 1. Ozone is also elevated, perhaps indicative of ozone production.

Between the second interception of point B and point D, the aircraft descended through air with higher θ_e and lower levels of ozone, ethane and CO. Relative humidity was 100% on this descent, indicative of convection mixing air from the cleaner side of the frontal surface below. Extrapolation of the profiles upwards from below 1.7 km to the level of descent between B and D appears to be consistent with this hypothesis.

Below 1.4 km, the CO and ethane were again higher, while there was negligable sulfate aerosol. The cross–section (Fig. 12b) shows that back trajectories in the lowest layer ahead of the warm sector originated where θ_e was very low. The 7 day trajectories descend from around 600 hPa over Hudson Bay and enter the Atlantic boundary layer 2 days before arrival where they experience rapid increase in θ_e associated with moistening and warming so that their θ_e signature is lost. It is likely that the CO and hydrocarbons are associated with the accumulation of forest fire emissions over northern Canada [*Pfister et al.*, 2005].

The top of the profile at point C is also influenced by forest fire emissions into air that had descended from near tropopause level over Canada. These fire emissions were encountered wherever the flight crossed the low θ_e layer (green) in Fig. 12b. The profiles down and up through the fire layer near F revealed that CO was highest near the bottom of the layer (150 ppbv) but near the top there was a dry layer with higher ozone. Very similar characteristics were observed by the BAe146 on 31 July – at this earlier time the top layer contained ozone up to 200 ppbv, implying that the fire emissions had mixed with stratospheric air across the tropopause somewhere upwind. Point F also has coincident matches with the WP3-D on 28 July when it intercepted the fire plume north of the St. Lawrence River (yellow trajectories in Fig. 9b). This flight also showed clear evidence of earlier mixing of emissions into stratospheric air.

6.2. Observed hydrocarbon fingerprints

The Lagrangian cases were identified on the basis of coincident matches where samples with similar hydrocarbon fingerprints are linked by matching trajectories and/or FLEXPART model matches. Figure 14 shows the hydrocarbon fingerprints from all the flights linked in each case. For each sample, ratios of hydrocarbons relative to ethane are found, h_i, and then these are adjusted to account for loss by reaction with OH using Eqn (1) to the time of the designated reference flight for that case (see last column of Table 1). The flight linked with the most other flights, or the furthest upwind was chosen as the reference. The ratios are decreased for flights occurring before the reference time and increased for flights occurring after the reference time. Note that the rate coefficients, k_i, have a weak temperature and pressure dependence which is accounted for using observed temperature and pressure at the sample locations and interpolating linearly between them. This explains for the slight differences in k_i between samples in Fig. 14, even for the same hydrocarbon. Vertical lines link points corresponding to the same species if they are widely spaced.

In the scenario of a pollution plume experiencing oxidation and mixing with a dilute background, the OH-adjusted ratios for the samples in each case should be indistinguishable. The spread between linked samples is much less than randomly selected samples and also much less than the variability between species, although the spread between samples increases with reactivity. Therefore, each case has a distinct hydrocarbon fingerprint and the linked flights did indeed sample almost the same air mass.

Note that the alkene (ethene and propene) concentrations have not been adjusted for OH reaction before calculating their ratios. This is because their ratios are not observed to decrease rapidly, as would occur from OH loss alone. Indeed, in Cases 4 and 5 the alkene ratios are found to be almost the same downwind as upwind. This behaviour may point to alkenes being involved as short-lived intermediates in the degradation of higher hydrocarbons and merits further investigation.

For Case 1: the DC8 ratios are systematically higher than observed by the BAe146 or Falcon downstream. This can be accounted for by assuming a higher average OH concentration than 1×10^6 molec cm^{-3} for this case. *Arnold et al.* [2006] find an optimum OH in this case of $2 - 3 \times 10^6$ molec cm^{-3}. During transit across the Atlantic this air mass was just above the boundary layer with high specific humidity and under clear skies, together conducive to high OH.

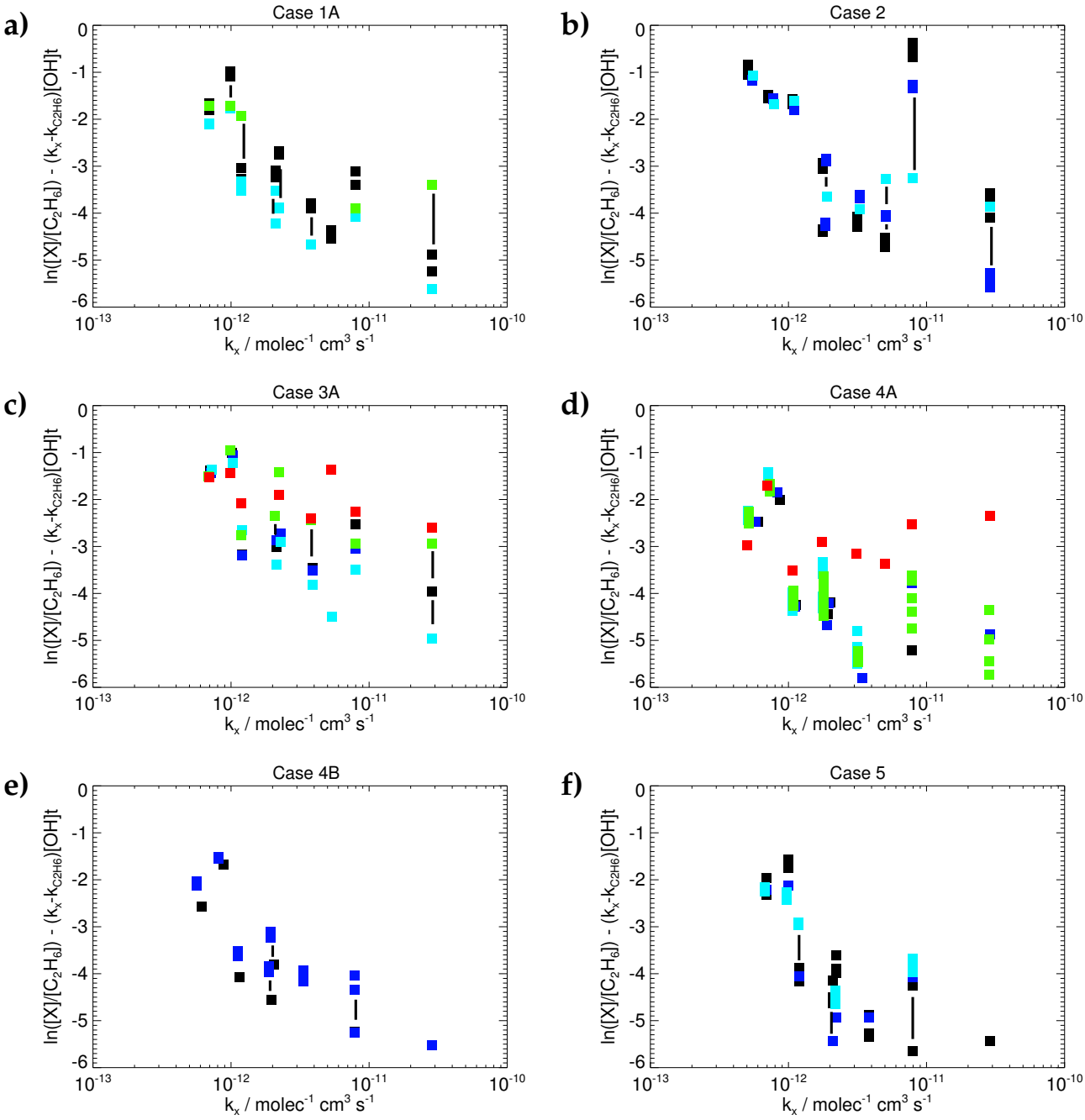

Figure 14. Ratios of hydrocarbon concentrations to ethane, adjusted for loss by reaction with OH, plotted against the rate coefficient, k_x. In order of increasing k_x the species are: acetylene, propane, benzene, iso-butane, *n*-butane, pentane, hexane, ethene and propene. A uniform OH concentration of 10^6 molec cm^{-3} is assumed. Note that ethene and propene ratios are not adjusted for OH loss (see text for discussion). The flights in each case are coloured in time-order as shown in Table 1: 1–black, 2–dark blue, 3–pale blue, 4–green, 5–red.

Case 2: exhibits the highest correlation statistic, r (2). It is readily identified as the Alaskan fire plume by the extreme concentrations of hydrocarbons and CO. It also has a fingerprint that contrasts with the anthropogenic pollution cases: acetylene, benzene and particularly ethene are high relative to alkanes. Iso-butane is present in much lower concentration than *n*-butane, while the difference is less in anthropogenic cases. Note that the spread in observed ethene ratios can be reduced by considering OH loss (the OH-adjusted ratios are very similar), indicating that ethene production from higher hydrocarbons does not counter-balance OH loss in this fire plume, in contrast to the anthropogenic pollution cases.

For Case 3: the OH-adjusted Falcon ratios are generally highest. This difference can be reduced by assuming a lower OH concentration than 1×10^6 molec cm^{-3}. This is consistent with the observation that this air mass was cloudy during its transit across the Atlantic. Although originating

from a similar portion of East Coast USA, the hydrocarbon fingerprint is quite different to Case 1. Acetylene, benzene, butane and pentane are significantly higher relative to ethane. Note that the Falcon flight over the English Channel on 26 July (red squares) was found to have much higher ratios for the short-lived hydrocarbons (especially hexane), indicating the influence of fresh emissions. Fresh emissions were also detected in NO_x.

In Case 4A: the flights match closely except the Falcon on 31 July (red squares). For this flight the long-lived species match (acetylene, propane, benzene) but the short-lived species are present with much higher concentrations. The trajectories matching the BAe146 and Falcon (red in Fig. 9a) do not link well with the trajectories matching the DC8 and WP3-D flights with the BAe146. They shadow the other coincident trajectories between the USA and Azores, but at a slightly lower altitude. However, this altitude displacement cannot account for the greater hydrocarbon ratios because in Case 5 air with similar geographical origin (red trajectories in Fig. 9b) that is exported at low levels has a similar hydrocarbon fingerprint to the other samples in Case 4A. It is most likely that the air mass was modified by convective mixing over Europe. Convection did not occur over Southern England on 31 July, but was present over northern France and Belgium and presumably brought some fresh European emissions to the flight level.

Case 4B: links the DC8 on 25 July with the BAe146 on 29 July when it was to the north of the line convection along the front. The trajectories (green in Fig. 9a) are similar to those for Case 4A (although they link different flight segments) and the hydrocarbon fingerprint is very similar. The systematic offset in ratios between the DC8 and BAe146 can be reduced if lower OH than 1×10^6 molec cm^{-3} is assumed. *Arnold et al.* [2006] investigates the OH concentration required to optimise matches in each Lagrangian case.

Case 5: links the WP3-D flying just off Pease on 28 July with two flights of the BAe146 intersecting the air mass in the lower troposphere just behind a front in the mid-Atlantic. The air was over the East Coast USA at the same time as the air in Case 4, but at lower altitudes. It has a similar hydrocarbon fingerprint, but is higher in acetylene and ethene and considerably lower in butanes. Another interesting observation is that the benzene/ethane ratio was much higher on 1 August than 31 July, while the propane/ethane ratio was lower. This is not inconsistent with mixing over the intervening day between the anthropogenic low level export (as seen by WP3-D on 28 July) and the fire layer above in the frontal zone (Fig. 12b), assuming that the fire layer has a fingerprint similar to Case 2. A similar argument may also explain the higher benzene/ethane ratio seen by the Falcon on 22 July in Case 1A, since the anthropogenic (high sulfate) layer was overlain by a fire layer on this day too.

6.3. Observed composition change following air masses

The tracer characteristics observed during the time windows linked by the Lagrangian cases are shown in Table 1. The mean and standard deviation has been calculated using 1s data over the time windows. The number of whole air samples collected during each window is also indicated. The penultimate column shows the PAN concentration measured by the DC8, WP3-D and BAe146. For the DC8 cases over short time-windows the measurement for the sum of PNs is shown because it was made at higher frequency than PAN. The Falcon did not measure PAN, but total reactive nitrogen (NO_y) was measured. The DC8 and WP3-D also measured NO_y but the BAe146 NO_y measurement unfortunately did not produce results during ICARTT. In the upper level Cases 2 and 4, most of the NO_y was in the form of PAN, while at low levels (Cases 1, 3 and 5) PAN is a much smaller fraction of NO_y as a result of thermal decomposition.

The last column shows the "growth rate" of CO over the intervals linking each flight segment with the designated reference flight for that case. The growth rate is always calculated forwards in time, such that a negative value indicates CO decrease. Most of the decrease can be attributed to mixing with more dilute neighbouring air masses, since CO photochemical loss is so slow.

In Case 1A: the DC8 and WP3-D match windows were separated by less than an hour and 0.35° latitude on their descent into Pease from the west. The hydrocarbon fingerprint observed by the DC8 (Fig. 14a) closely matches that observed by the BAe146 on 19 July and the Falcon on its level run at 913 hPa. Unfortunately, the WP3-D did not collect hydrocarbon samples due to a system failure. The WP3-D was at slightly lower altitude (887 hPa compared with DC8 window-average of 855 hPa) where CO and ozone were higher. PAN was not measured by the DC8 on this descent, but almost 1 ppbv was observed by the WP3-D.

Closer inspection reveals that the CO concentration increased during the continuing descent of the DC8 to around 190 ppbv in a dry layer (RH≈90%) with maximum NO, just above the local saturated boundary layer. This more polluted layer (at 902 hPa) has a coincident match with the BAe146 on 25 July, rather than 19 July, and forms Case 1B. Its hydrocarbon fingerprint (not shown) is similar to Case 1A but with higher propane/ethane and butane/ethane ratios. It is likely that the Case 1A and Case 1B air masses picked up emissions further west, as indicated by the very high sulfate aerosol concentrations thought to originate in the Ohio River Valley, but that only the lower Case 1B air mass was influenced by fresh emissions from the cities on the East Coast. This layer matches with the Falcon on a lower run at 965 hPa which was observed to have higher CO and NO_y than the Case 1A match-window.

Another segment along the WP3-D track which has trajectory and FLEXPART matches with the Falcon and BAe146 is further south by about 100 km (near Cape Cod). Unfortunately, there were no hydrocarbon samples from the WP3-D, but the trajectories from this segment shadow the red trajectories in Fig. 2b very closely. Here the WP3-D crossed the maximum in the plume downwind of the New York conurbation (level at 928 hPa) and clearly observed higher CO and ozone than the DC8 closer to Pease.

Potential temperature varies little following the air mass 1A, but initially θ_e decreases, consistent with a decrease in specific humidity while maintaining constant temperature between Pease and the BAe146 on 19 July (as occurs in Case 3). After this θ_e is well conserved. The CO mixing ratio decreases with time but at a surprisingly slow rate indicating a dilution timescale in the range 15-25 days (although it would be faster if the WP3-D were used as the reference). This is consistent with the profile observed by the BAe146 (Fig. 5) which shows the persistence of layering within the target air mass as it rides above the marine boundary layer with hardly any influence from below. The surrounding air masses also have elevated CO, so that the

Table 1. Measurements taken during Lagrangian match windows defined by the times t_{start} and t_{end} in days since 00UT 1 Jan 2004. The flights legs are labelled P for profile or L for level, or both. The number of hydrocarbon samples is given. Data for each window is shown as "mean (standard deviation)". $^{\dagger}NO_y$ is shown rather than PAN for the Falcon. ‡PNs measurement is shown rather than PAN in some DC8 cases. The last column shows the "growth rate" for CO between the flight in that row and the reference flight for the Lagrangian case.

Flight	t_{start} (day)	t_{end} (day)	Leg	WAS	θ (K)	θ_e (K)	CO (ppbv)	O_3 (ppbv)	PAN (pptv)	$\frac{\Delta(\ln[CO])}{\Delta t}$ (day^{-1})
Case 1A: USA to Portugal (low level)										
15 Jul DC8	197.84375	197.84506	P	2	299.0 (1.4)	329.0 (1.0)	147.4 (12.3)	59.1 (1.7)	-	ref
15 Jul WP3-D	197.87292	197.87875	L	0	298.7 (0.4)	330.6 (0.7)	166.4 (10.8)	69.1 (1.6)	901 (142)	-
19 Jul BAe146	201.54081	201.54868	L	2	296.2 (0.5)	321.5 (0.5)	125.4 (2.8)	60.5 (1.9)	33 (15)	-0.044 (0.023)
22 Jul Falcon	204.52851	204.53256	L	1	295.7 (0.2)	319.1 (0.7)	106.0 (1.1)	46.4 (0.7)	†400 (14)	-0.049 (0.013)
Case 1B: USA to Portugal (lowest level)										
15 Jul DC8	197.84506	197.84771	L	4	296.9 (0.7)	331.7 (0.3)	183.2 (6.1)	60.9 (4.7)	-	ref
15 Jul WP3-D	197.85916	197.86333	L	0	298.2 (0.5)	332.3 (0.9)	203.3 (6.2)	80.2 (1.8)	1107 (215)	-
22 Jul Falcon	204.54167	204.54720	L	1	293.4 (0.2)	321.4 (1.2)	111.4 (1.3)	42.0 (1.0)	†470 (31)	-0.074 (0.005)
25 Jul BAe146	207.77020	207.77367	L	1	300.7 (0.2)	322.8 (1.0)	83.0 (2.9)	32.9 (2.2)	9 (2)	-0.080 (0.005)
Case 2: Alaskan fire plume (upper level)										
18 Jul DC8	200.77740	200.79333	L	3	319.4 (0.3)	320.2 (0.2)	448.7 (68.0)	61.6 (2.6)	‡2228 (413)	ref
20 Jul BAe146	202.51820	202.52208	L	3	319.0 (0.1)	320.1 (0.1)	415.4 (49.1)	67.5 (1.2)	2672 (296)	-0.044 (0.110)
23 Jul Falcon	205.54083	205.55042	L+L	1	314.0 (0.9)	319.4 (1.4)	242.5 (34.9)	78.9 (3.6)	†1960 (245)	-0.129 (0.044)
Case 3: USA to Ireland (low level)										
21 Jul WP3-D	203.75292	203.75486	L+P	1	298.6 (0.3)	337.7 (1.9)	171.1 (8.6)	57.7 (3.4)	238 (17)	ref
22 Jul DC8	204.73950	204.74057	P	1	298.5 (0.6)	335.7 (0.6)	193.9 (1.4)	52.4 (0.4)	108 (-)	0.127 (0.051)
22 Jul WP3-D	204.74109	204.74583	L	1	297.0 (0.2)	334.0 (1.3)	174.9 (7.6)	51.4 (1.8)	238 (28)	0.022 (0.067)
25 Jul Falcon	207.66328	207.66733	L	1	293.9 (0.5)	318.6 (1.5)	149.1 (6.4)	41.3 (1.2)	†179 (6)	-0.035 (0.017)
26 Jul Falcon	208.71583	208.72222	L	1	294.5 (0.4)	316.7 (0.6)	121.0 (1.8)	42.6 (1.5)	†924 (422)	-0.070 (0.011)
Case 4A: Upper level export by frontal system										
25 Jul DC8	207.77257	207.77384	P	1	315.1 (0.8)	330.0 (2.6)	104.4 (4.6)	61.6 (2.4)	‡292 (30)	-0.003 (0.017)
27 Jul WP3-D	209.68229	209.68634	L	1	317.6 (0.1)	338.9 (0.4)	96.7 (8.6)	67.0 (1.4)	395 (49)	0.036 (0.055)
28 Jul DC8	210.78584	210.79626	L	5	336.4 (0.2)	338.5 (0.2)	113.0 (4.9)	70.9 (3.0)	567 (64)	-0.123 (0.088)
29 Jul BAe146	211.51750	211.53125	L+P	5	334.5 (1.1)	337.9 (1.0)	103.3 (4.9)	70.4 (6.0)	572 (91)	ref
31 Jul Falcon	213.52277	213.52571	P+L	1	331.3 (1.0)	-	85.3 (1.4)	78.9 (5.4)	†663 (56)	-0.095 (0.025)
Case 4B: Upper level export by frontal system										
25 Jul DC8	207.75173	207.75289	P	1	318.6 (1.4)	336.5 (0.6)	106.0 (3.2)	67.5 (5.5)	‡341 (68)	ref
29 Jul BAe146	211.53343	211.54292	L	3	335.7 (0.5)	338.1 (0.5)	111.0 (2.2)	79.9 (5.0)	643 (33)	0.011 (0.010)
Case 5: Low level export by frontal system										
28 Jul WP3-D	210.83333	210.84410	L	3	304.7 (0.1)	333.2 (1.8)	98.4 (7.8)	62.3 (3.8)	185 (28)	ref
31 Jul BAe146	213.48375	213.48917	P	1	302.0 (1.7)	330.0 (1.0)	94.6 (3.2)	51.6 (3.0)	56 (27)	-0.015 (0.033)
1 Aug BAe146	214.48583	214.49167	L	3	301.8 (0.3)	324.0 (0.7)	97.7 (2.5)	48.8 (3.2)	18 (5)	-0.002 (0.023)

CO-contrasts are weak and CO decrease would be slow even if turbulent mixing was quite active.

Ozone is seen to systematically decrease following both air masses. Using Lagrangian photochemical models initialised with the composition observed by the WP3-D, the rate of ozone decrease can be accounted for by photochemical loss in the humid air mass (Arnold, personal communication; *Whalley et al.* [2006]) even without allowing for any contact with the marine boundary layer and ocean surface below. However, the DC8 match-windows have significantly lower ozone and CO indicating slower ozone loss. Entrainment from the polluted layer (1A) into the marine boundary layer would also help maintain higher ozone (and sulfate aerosol) there. In a similar situation with overlying pollution during the ACE-2 Lagrangian case 3 [*Wood et al.*, 2000], the marine boundary layer aerosol was observed to evolve very little over 30 hours. It is likely that the composition observed downwind by the Falcon and BAe146 represents a mix of air with composition similar to that observed by the WP3-D and DC8 on 15 July. This case highlights the difficulties introduced by strong gradients, especially in the vertical, close to source and assumptions on mixing across these gradients. The WP3-D flight crossed horizontal and vertical edges of the pollution plume several times and more detailed analysis would be required to determine suitable initial conditions and treatment of mixing for photochemical models.

Case 2: follows the Alaskan fire plume descending in the upper troposphere. θ_e hardly varies between interceptions. CO is extremely variable within the air mass, although the variability decreases with time. The timescale for mixing inferred from the CO decrease between the DC8 and Falcon exceeds 6 days, which is shorter than inferred from the other cases. However, in this case the plume is very concentrated relative to its surroundings, so that the jump in CO across its edges is almost as much as the mixing ratio within the plume. Therefore, the higher rate of CO decrease does not imply that turbulent mixing is stronger in this case.

Ozone increases significantly following this air mass. *Whalley et al.* [2006] and *Real et al.* [2006] show that Lagrangian photochemical models initialised with the DC8 observations can account for this increase, although when mixing is parameterised the modelled ozone increase falls short. However, the average PAN observed by the BAe146 is higher than observed by the DC8 indicating that the Lagrangian match is not perfect. The BAe146 flew through the plume maximum on a slightly different level relative to the air mass sampled upstream by the DC8. The maximum CO observed by the BAe146 during the match window was 537 ppbv which was less than the maximum observed by the DC8 (613 ppbv). However, CO was significantly lower for the second half of the DC8 match window, bringing down the mean, and perhaps less well linked with the BAe146.

Case 3: followed a well-defined, slowly moving plume on three consecutive days, just above and within the boundary

layer, from the New York urban area, across the Gulf of Maine and Nova Scotia. Smart balloons were also released into the air mass [*Riddle et al.*, 2006], tracking it throughout this period. The pollution was situated on the northern flank of a warm conveyor belt bringing moist, warm (high θ_e) air along the eastern seaboard of the USA. The WP3-D flight on 21 July zig-zagged across the pollution plume 3 times while flying towards the northeast. CO, hydrocarbon and PAN concentrations were much greater (CO peaking at 350 ppbv) on the lowest level runs (980 hPa) and at the upstream end (east of Cape Cod). The coincident matches with the Falcon were found on the northern flank of the plume near its top edge and therefore much lower concentrations are shown in Table 1.

CO decreases with time between the WP3-D on 22 July and the Falcon on 25 July, although at a surprisingly slow rate. Although the DC8 flight indicates higher CO, it was displaced relative to the target air mass (see Fig. 6b). The DC8 also observed half the PAN seen by the WP3-D on 22 July. Mixing between the air mass matching the Falcon and more polluted portions of the plume below and to the south must be considered carefully for this case. In particular, the Falcon observed much higher butane/ethane ratios to the west of Ireland than the WP3-D or DC8 observed in the match-windows on 21 and 22 July (Fig. 14c). However, higher ratios were observed on the WP3-D flights within the plume centre, indicating that mixing occurred with this air after 22 July during transit across the Atlantic.

A prominent feature of Case 3 is that θ_e decreases a great deal between the WP3-D close to Nova Scotia and the Falcon near Ireland, while θ is almost unchanged. The air mass was not intercepted over the mid-Atlantic but analysed temperature and humidity interpolated from the ECMWF model to the trajectories (shown in Fig. 6b) indicates that humidity decreased along the entire trajectory with greatest θ_e-decrease during the poleward movement towards Greenland. The WP3-D flights on 21 and 22 July observed a dry layer with lower θ_e but slightly higher θ immediately above the polluted target. Continuous entrainment from above into the polluted air mass could explain the humidity decrease while maintaining potential temperature. The smart balloons observed heating during daytime and cooling at night, but no overall cooling crossing the Gulf of Maine. Cloud was observed by satellite following the trajectory northwards which would inhibit radiative cooling. Additionally, the air mass was part of a warm sector originating far to the south with high θ_e. Therefore, sea surface temperature beyond Nova Scotia was always much cooler than the air which would inhibit convection within the marine boundary layer. Owing to weak turbulent fluxes, moisture would not be re-supplied to the air mass from the ocean fast enough to offset entrainment of dry air from above.

As with Case 1, ozone decreases following the air mass until 25 July, despite the pollution. On 26 July the Falcon intersected the air mass over the English Channel. However, NO_y was strongly elevated in a narrow spike during the match window with a large fraction in the form of short-lived NO_x. This spike is clearly indicative of fresh emissions, probably from southern England, and accounts for the high mean and standard deviation in NO_y. The fresh emissions also elevated the short-lived hydrocarbon content and disrupted the fingerprint (red symbols in Fig. 14c).

The long-term record at Mace Head on the west coast of Ireland shows that CO as high as 100 ppbv is rare when air approaches from the west - most pollution episodes there are associated with air from the rest of Europe to the east [*Derwent et al.*, 1998]. It is uncommon for large-scale plumes from the USA to travel within the boundary layer and lower troposphere on such a northerly trajectory. More frequently low level export heads towards the Azores, as observed at Pico [*Helmig*, 2006]. Usually, air heading northeastwards from the USA and then curving round to Europe is associated with strong ascent along the East Coast USA within warm conveyor belts and the outflow crosses western Europe in the upper troposphere [*Eckhardt et al.*, 2004].

Case 4: is an example of such ascent and upper level export associated with a warm conveyor belt, although the ascent is weaker in summer than other seasons [*Eckhardt et al.*, 2004]. Potential temperature increases by 20 K, associated with latent heat release, while θ_e is conserved. CO is more variable between the matching windows than within each window indicating that the Lagrangian matches are not perfect. The DC8 on 28 July and BAe146 on 29 July are most closely linked and clearly CO decreases with time over this day. PAN and ozone are indistinguishable between these match windows. Note that the DC8 on 28 July observed total PNs concentrations of 606 (64) pptv, implying that 94% of PNs was in the form of PAN. The slightly lower CO observed earlier by the DC8 on 25 July and WP3-D on 27 July may indicate simply a displacement relative to the air mass seen by the BAe146 or mixing of further CO into the air mass by convection over the USA (as discussed by *Cooper* [2006]) after these upwind intersections. Ozone was extremely uniform within each match window and increases with time following the air mass, indicative of photochemical production. PAN also increases as the air mass ascends between the 25 July and 28 July, consistent with conversion from NO_x. Figure 14d shows that the air sampled by the Falcon on 31 July had been recently influenced by fresh emissions from Europe. In addition, two spikes in NO were observed during the match window with an NO/NO_y ratio just above 10%. However, the NO_y is not much greater than the upstream PAN observations, consistent with a Lagrangian match and the assumption that most NO_y is in the form of PAN in the upper troposphere.

Case 5: follows air exported at low levels during the same frontal passage across East Coast USA that resulted in the upper level export observed in Case 4. The observations occur on the same potential temperature surface, although θ_e decreases slightly with time. This could be explained by weak mixing between the high θ_e of the polluted air mass and the very low θ_e of the cold, dry layer immediately above the frontal surface (see Fig. 12b). CO barely changes with time. This is not surprising when it is realised that the cold, dry layer above contains high CO from the boreal fires over Northern Canada, so that the CO-gradients between the air masses are very slack (Fig. 13). An increase in benzene/ethane ratio (a characteristic of fire plume Case 2) between 31 July and 1 August supports the hypothesis of mixing with the fire layer. PAN decreases with time associated with thermal decomposition. Ozone decreases with time, but modelling studies are required to determine the contribution from photochemical loss.

7. Conclusions

Evidence has been presented to demonstrate that air masses were sampled several times during transit across the

North Atlantic as part of the ICARTT-Lagrangian experiment. Many Lagrangian matches were identified objectively using a novel technique that combines Lagrangian trajectories, calculated using global meteorological analyses, and the hydrocarbon fingerprints analysed from whole air samples collected by the aircraft. Five cases were identified with strong links between at least three flights spanning the Atlantic. The variability between the hydrocarbon fingerprints of linked samples is very small compared to the differences between randomly selected samples, once the loss of hydrocarbons through OH reaction over the time between samples is accounted for. The relationships between the longer-lived hydrocarbons are particularly close, with variability comparable to the variability between samples collected on one flight through the same air mass.

There is always uncertainty concerning the closeness of the Lagrangian matches. The ideal situation would be for the differences between downwind and upwind interceptions of an air mass to reveal photochemical transformation in composition. However, two factors render this task difficult:

1. Variability within an air mass, since the upwind and downwind aircraft may sample the air mass differently, even if its structure and composition had not changed over the interval between flights. For example, in Case 2, following the Alaskan fire plume, there was strong variability in CO and the DC8 and BAe146 spent a different fraction of time near the CO maximum. There is also uncertainty in the vertical structure of the shallow plume and the level of the aircraft relative to the plume maximum. However, other tracers, that are not directly emitted from the fires, are much more uniform. For example, equivalent potential temperature agrees to within 1 K between the interceptions of the DC8, BAe146 and Falcon through the plume. Since ozone variability is small within the plume it is reasonable to suggest that the downwind minus upwind differences are a good estimate of ozone evolution.

2. Mixing by turbulence following the flow resolved in atmospheric analyses. In the Lagrangian experiment, the rate of mixing was not observed between interceptions and the gradients with neighbouring air masses, which change continuously, were also not sampled between flights. The only quantitative way to partition the observed change between photochemical reaction and physical processes is through the use of a model.

Bearing these limitations in mind, the quality of different matching techniques was assessed using independent observations of tracers to find downwind minus upwind differences. The distribution of θ_e-differences for trajectory-only or hydrocarbon-only matches was much more strongly peaked about zero than pairing random time points drawn from the same set of flights. Importantly, when the information was combined in the search for "coincident matches" the peak of the PDF more than doubled, showing that the quality of these matches was much higher. With the exception of the coincident trajectories in Case 3, the θ_e-differences almost all lie within ± 2 K as expected for a pseudo-adiabatic process following an air mass. Potential temperature increase shows that some of these coincident matches experienced latent heat release associated with ascent and condensation. In addition, the PDFs were almost identical when using the UGAMP trajectory model or FLEXPART Lagrangian dispersion model, together with hydrocarbon fingerprints, to identify matches. This indicates that the quality of the matches identified using two different models, with different trajectory matching criteria, are similar even though there are differences in the match windows highlighted.

The PDF of CO growth rate (defined by (3)) shows CO increase for a few matches, either indicating a mismatch or mixing of more CO into the air mass. However, in the vast majority of cases there is slow CO decrease. If the loss rate is associated with a mixing timescale it appears to be very long (10-20 days for 38% of matches). However, the CO decreases so slowly because the CO in neighbouring air masses is usually a large fraction of the CO in the target air mass.

The PDF of ozone growth rate peaks at slow increase, although there is a clear second peak on weak decrease. It is not possible to quantify the proportion associated with photochemistry, as opposed to mixing, without running a photochemical model for all matches.

The best five Lagrangian cases (see Table 1) cover a variety of situations. Cases 1, 3 and 5 followed anthropogenic pollution at low levels from the East Coast USA right across the Atlantic. Case 3 was clearly influenced by entrainment from a dry layer overlying the pollution (below 850 hPa). Nevertheless, mixing was slow and layering and strong variability in CO was still observed by the Falcon just west of Ireland. Case 1 also retained a highly stratified structure with weak mixing and virtually no shear in the flow. Two distinct air masses were identified travelling one above the other, the lower of which (Case 1B) was influenced by fresh emissions close to the US East Coast. The upper layer (1A) travelled just above the marine boundary layer and appeared to mix very slowly with its neighbours, while the lower layer (1B) descended slowly into the marine boundary layer. Continuous, but slow, entrainment from the polluted low level outflow into the marine boundary layer helped to maintain high pollutant levels (e.g., sulfate aerosol) there as observed in Lagrangian case 3 of ACE-2 [*Wood et al.*, 2000]. Ozone decrease occured in air masses travelling at low level, even if well above the boundary layer (e.g., Case 5 following a cold front). Case 2 followed a fire plume originating from fires in Alaska as it descended from the upper troposphere across the Atlantic. Case 4 followed air ascending from Southeast USA in a warm conveyor belt and then across the Atlantic in the upper troposphere. Ozone increase occurs in the upper troposphere in anthropogenic pollution and the Alaskan fire plume.

The cases detailed in this paper provide a basis for detailed chemical transport modelling studies constrained by observations. It is hoped that changes in concentrations of compounds that are not routinely observed, such as higher hydrocarbons, alkyl nitrates and PNs will reveal exciting new information about photochemical pathways.

Acknowledgments. Thanks to the whole of the ICARTT team: the scientists, pilots and support staff associated with all the measurement platforms and their campaign bases. The Natural Environment Research Council (NERC) funded the ITOP-UK project and flying time as part of the Upper Troposphere– Lower Stratosphere Ozone (UTLS) thematic programme. The ITOP-UK team would also like to give heartfelt thanks to the dedication of the staff from the Facility for Airborne Atmospheric Measurements and in particular, John Reid, without whom the BAe146 would never have reached the Azores, let alone made measurements, on its first deployment. The deployment of the DLR Falcon in Creil, France was funded by DLR. French participation in European ITOP was funded by Programme National de Chimie Atmosphérique (PNCA) (ADEME, Agence gouvernementale de l'Environnement et de la Maitrise de l'énergie)/PATOM (Programme Atmosphère et Océan Multi-échelles) of INSU (Institut

National des Sciences de l'Univers) and IPSL (Institut Pierre Simon Laplace). Local support from IGN (Institut Géographique National), Creil is gratefully acknowledged. John Methven is grateful for support through an Advanced Fellowship jointly sponsored by NERC and the Environment Agency.

References

Arnold, S., et al., Inference of tropospheric OH and air mass dilution rates from the ICARTT Lagrangian experiment, *J. Geophys. Res.*, *this volume*, 2006.

Bates, T., B. Huebert, J. Gras, F. Griffiths, and P. Durkee, International Global Atmospheric Chemistry (IGAC) Project's first Aerosol Characterisation Experiment (ACE-1): Overview, *J. Geophys. Res.*, *103*, 16,297–16,318, 1998.

Cooper, O., Large upper tropospheric ozone enhancements above mid-latitude North America during summer. In situ evidence from the IONS and MOZAIC monitoring network., *J. Geophys. Res.*, *this volume*, 2006.

Derwent, R., P. Simmonds, S. Seuring, and C. Dimmer, Observation and interpretation of the seasonal cycles in the surface concentrations of ozone and carbon monoxide at Mace Head, Ireland from 1990 to 1994, *Atmos. Environ.*, *32*, 145–157, 1998.

Eckhardt, S., A. Stohl, H. Wernli, P. James, C. Forster, and N. Spichtinger, A 15-year climatology of warm conveyor belts, *J. Climate*, *17*, 218–237, 2004.

Esler, J., D. Tan, P. Haynes, M. Evans, K. Law, P. Plantevin, and J. Pyle, Stratosphere-troposphere exchange: Chemical sensitivity to mixing, *J. Geophys. Res.*, *106*, 4717–4731, 2001.

Esler, J., G. Roelofs, M. Köhler, and F. O'Connor, A quantitative analysis of grid-related systematic errors in oxidising capacity and ozone production rates in chemistry transport models, *Atmos. Chem. Phys.*, *4*, 1781–1795, 2004.

Fehsenfeld, F., ICARTT overview, *J. Geophys. Res.*, p. this volume, 2006.

Fitzgerald, J., J. Marti, W. Hoppel, G. Frick, and F. Gelbard, A one dimensional sectional model to simulate multicomponent aerosol dynamics in the marine boundary layer. (2): Model application, *J. Geophys. Res.*, *103*, 16,103–16,117, 1998.

Forster, C., et al., Transport of boreal forest fire emissions from Canada to Europe, *J. Geophys. Res.*, *106*, 22,887–22,906, 2001.

Frost, G., et al., Effects of changing power plant NOx emissions on ozone in the Eastern United States, *J. Geophys. Res.*, *submitted*, 2005.

Good, P., C. Giannakopoulos, F. O'Connor, S. Arnold, M. de Reus, and H. Schlager, Constraining tropospheric mixing timescales using airborne observations and numerical models, *Atmos. Chem. Phys.*, *3*, 1023–1035, 2003.

Guenther, A., et al., A global model of natural volatile organic compound emissions, *J. Geophys. Res.*, *100*, 8873–8892, 1995.

Haynes, P., and J. Anglade, The vertical-scale cascade in atmospheric tracers due to large-scale differential advection, *J. Atmos. Sci.*, *54*, 1121–1136, 1997.

Helmig, D., Seasonal photochemistry and air transport in the North Atlantic Region as inferred from NMHC measurements at Pico Mountain, Azores, *J. Geophys. Res.*, *this volume*, 2006.

Hoell, C., C. O'Dowd, S. Osborne, and D. Johnson, Timescale analysis of marine boundary layer aerosol evolution: Lagrangian case studies under clean and polluted cloudy conditions, *Tellus*, *52B*, 423–438, 2000.

Huebert, B., A. Pszenny, and B. Blomquist, The ASTEX/MAGE experiment, *J. Geophys. Res.*, *101*, 4319–4329, 1996.

Jobson, B., D. Parrish, P. Goldan, W. Kuster, F. Fehsenfeld, D. Blake, N. Blake, and H. Niki, Spatial and temporal variability of nonmethane hydrocarbon mixing ratios and their relation to photochemical lifetime, *J. Geophys. Res.*, *103*, 13,557–13,567, 1998.

Johnson, D., S. Osborne, R. Wood, K. Suhre, R. Johnson, and S. Businger, An overview of the Lagrangian experiments undertaken during the North Atlantic regional Aerosol Characterization Experiment (ACE-2), *Tellus*, *52B*, 290–320, 2000.

Kleissl, J., The occurrence of upslope flows at Pico mountaintop observatory: a case study of orographic flows on small, volcanic islands, *J. Geophys. Res.*, *this volume*, 2006.

Legras, B., B. Joseph, and F. Lefevre, Vertical diffusivity in the lower stratosphere from Lagrangian back trajectory reconstructions of ozone profiles, *J. Geophys. Res.*, *108*, 4562, doi:10.1029/2002JD003,045, 2003.

Lehmann, R., P. von der Gathen, M. Rex, and M. Streibel, Statistical analysis of the precision of the Match method, *Atmos. Chem. Phys.*, *5*, 2713–2727, 2005.

Lewis, A., ITOP-UK overview, *J. Geophys. Res.*, *this volume*, 2006.

Methven, J., Offline trajectories: Calculation and accuracy, *Tech. Rep. 44*, U.K. Univ. Global Atmos. Modelling Prog., Dept. of Meteorol., Univ. of Reading, U.K., 1997.

Methven, J., and B. Hoskins, The advection of high resolution tracers by low resolution winds, *J. Atmos. Sci.*, *56*, 3262–3285, 1999.

Methven, J., S. Arnold, F. O'Connor, H. Barjat, K. Dewey, J. Kent, and N. Brough, Estimating photochemically produced ozone throughout a domain using flight data and a Lagrangian model, *J. Geophys. Res.*, *108(D9)*, 4271, doi:10.1029/2002JD002,955, 2003.

Olivier, J., A. Bouwman, J. Berdowski, C. Veldt, J. Bloos, A. Visschedijk, C. van der Maas, and P. Zandveld, Sectoral emission inventories of greenhouse gases for 1990 on a per country basis as well as on 1x1 degree, *Environmental Science and Policy*, *2*, 241–264, 1999.

Parrish, D., The effects of mixing on evolution of hydrocarbon ratios in the troposphere, *J. Geophys. Res.*, *this volume*, 2006.

Pfister, G., P. Hess, L. Emmons, J.-F. Lamarque, C. Wiedinmyer, D. Edwards, G. Petron, J. Gille, and G. Sachse, Quantifying CO emissions from the 2004 Alaskan wildfires using MOPITT CO data, *Geophys. Res. Lett.*, *32*, L11,809, doi:10.1029/2005GL022,995, 2005.

Prinn, R., R. Weiss, B. Miller, J. Huang, F. Alyea, D. Cunnold, P. Fraser, D. Hartley, and P. Simmonds, Atmospheric trends and lifetime of CH_3CCl_3 and global OH concentrations, *Science*, *269*, 187–192, 1995.

Raes, F., T. Bates, F. McGovern, and M. van Leide, The second Aerosol Characterisation Experiment (ACE-2): General overview and main results, *Tellus*, *52B*, 111–125, 2000.

Ravetta, F., Ozone LIDAR measurements, *J. Geophys. Res.*, *this volume*, 2006.

Real, E., et al., Processes influencing O_3 levels in Alaskan forest fire plumes during long-range transport over the North Atlantic, *J. Geophys. Res.*, *this volume*, 2006.

Rex, M., et al., In situ measurements of stratospheric ozone depletion rates in the Arctic winter 1991/1992: A Lagrangian approach, *J. Geophys. Res.*, *103(D5)*, 5843–5854, 1998.

Riddle, E., P. Voss, A. Stohl, D. Holcomb, D. Mazcka, K. Washburn, and R. Talbot, Trajectory model validation using constant altitude CMET balloons during ICARTT-2004, *J. Geophys. Res.*, *this volume*, 2006.

Roelofs, G., and J. Lelieveld, Model study of the influence of cross-tropopause ozone transports on tropospheric ozone levels, *Tellus*, *49B*, 38–55, 1997.

Stohl, A., S. Eckhardt, C. Forster, P. James, N. Spichtinger, and P. Seibert, A replacement for simple back trajectory calculations in the interpretation of atmospheric trace substance measurements, *Atmos. Environ.*, *36*, 4635–4648, 2002.

Stohl, A., O. Cooper, R. Damoah, F. Fehsenfeld, C. Forster, E.-Y. Hsie, G. Hübler, D. Parrish, and M. Trainer, Forecasting for a Lagrangian aircraft campaign, *Atmos. Chem. Phys.*, *4*, 1113–1124, 2004.

Stohl, A., C. Forster, A. Frank, P. Seibert, and G. Wotawa, The Lagrangian particle dispersion model FLEXPART version 6.2, *Atmos. Chem. Phys. Discuss.*, 2005.

Stohl, A., et al., A backward modeling study of intercontinental pollution transport using aircraft measurements, *J. Geophys. Res.*, *108 (D12)*, 4370, doi:10.1029/2002JD002,862, 2003.

Val Martin, M., Observations of large enhancements of nitrogen oxides in the North Atlantic lower troposphere resulting from boreal wildfires, *J. Geophys. Res.*, *this volume*, 2006.

Whalley, L., M. Evans, S. Arnold, and M. Pilling, Ozone production efficiency of an anthropogenic and biomass burning plume: Results from the 2004 ICARTT campaign, *J. Geophys. Res.*, *this volume*, 2006.

Wood, R., et al., Boundary layer and aerosol evolution during the 3rd Lagrangian experiment of ACE-2, *Tellus*, *52B*, 401–422, 2000.

J. Methven, Department of Meteorology, University of Reading, PO Box 243, Earley Gate, Reading, RG6 6BB. (J.Methven@reading.ac.uk)

S. R. Arnold, School of Earth and Environment, University of Leeds, Leeds, LS2 9JT, UK.

M. J. Evans, School of Earth and Environment, University of Leeds, Leeds, LS2 9JT, UK.

B. Rappenglück, Department of Geosciences, University of Houston, 4800 Calhoun Rd, Houston, TX 77204-5007, USA.

(Received _____.)